THE PENNSYLVANIA STATE UNIVERSITY
SCHREYER HONORS COLLEGE

DEPARTMENT OF PHYSICS

Improved Estimates for the Sensitivity of the Payload for Ultrahigh Energy Observations (PUEO) to Tau Neutrinos

DYLAN ESSEX MONTEIRO
SUMMER 2023

A thesis
submitted in partial fulfillment
of the requirements
for a baccalaureate degree
in Physics
with honors in Physics

Reviewed and approved* by the following:

Stephanie Wissel
Downsbrough Early Career Assistant Professor of Physics and Astronomy/Astrophysics
Thesis Supervisor

Richard Robinett
Professor of Physics
Honors Adviser

* Electronic approvals are on file.

ABSTRACT

Ultra-High Energy Neutrinos (UHEN) > EeV can serve as important probes of both astrophysics and particle physics in an unexplored energy scale. Unlike cosmic rays and gamma rays, UHEN can pass through large swatches of space without interaction, carrying unperturbed information from the edge of the observable universe. The Payload for Ultrahigh Energy Observations (PUEO) is a long duration balloon experiment designed to observe UHEN through radio detection. Particle showers caused by UHEN in ice and in Earth's atmosphere can produce radio signals through geomagnetic emission and Askaryan emission. Geomagnetic emission occurs through the separation of electrons and positrons along the shower due to Earth's geomagnetic field, while Askaryan emission occurs due to a negative charge excess on the shower front. To detect these signals, PUEO will have two primary detector arrays: the Main Instrument (MI) which consists of 256 horn antennas operating at 300-1200 MHz, and the Low Frequency (LF) Instrument which consists of 8 antennas operating at 50-300 MHz. Simulation studies have been ongoing to estimate the expected performance of the two instruments in their sensitivity to different UHEN signals. Computational efforts have made use of Monte-Carlo event generators in conjunction with detailed models of the various components of the antenna arrays. Results of one of these studies have led to design choices for the LF signal chain electronics. Additionally, a novel data transfer method interfacing two crucial components of the PUEO simulation system was designed and implemented to increase the accuracy of sensitivity predictions for the air shower channel. This method has been used to improve PUEO's tau neutrino sensitivity estimates as well as compare performance expectations between the two detectors.

TABLE OF CONTENTS

LIST OF FIGURES

Appendix

ACKNOWLEDGEMENTS

First and foremost, I would like to thank my supervisor Prof. Stephanie Wissel for her broad and thoughtful support for my career in physics. Besides accepting me to her group as a mentee, she continuously provided and searched for opportunities where I could advance my experience in academia. Through serving as a letter of recommendation writer and as a source of guidance she helped me get into a physics PhD program that I am tremendously excited for. Additionally, she motivated me to become a more prudent and meticulous researcher. This, in addition to her cultivation of an immensely inviting group culture, has contributed to my success as a physicist.

I would also like to thank my advisor Prof. Richard Robinett for his advice and keen eye for opportunities throughout my academic career. His suggestions for professors to pursue research with, in addition to guidance with honors classes helped me gain admission to the Schreyer Honors College. He has been the most attentive, communicative, and helpful academic advisor out of any of those of my peers.

Additionally, I am grateful for the assistance and contributions of Austin Cummings, who played a significant role in discovering the NaN noise described in Chapter 4 and analyzing the integration techniques between packages. Yuchieh Ku was also a great help in getting me started with the Wissel group and had significant contributions to the pueoSim LF instrument and TAPIOCA. I would also like to thank all the other members of PUEO and the Wissel group who have supported me and answered my multitude of questions about neutrino physics and simulation techniques.

I would like to thank my mother for always putting on Neil deGrasse Tyson shows and science documentaries for me as a child, and my father for attempting to answer my countless metaphysical questions that would result in lengthy discussions about the nature of reality. Their combined influence and support for my curiosity is a major reason I chose to begin a career in physics. Lastly, I would like to thank all of my friends who had to stand by, yet continued to support me while I worked on this thesis.

We gratefully acknowledge NASA Awards #80NSSC20K0775 and #80NSSC20K0925. The findings and conclusions of this thesis do not reflect the views of any funding agency.

1

Introduction

Because of neutrinos' extremely small cross section with nucleons, their lack of charge, and no known decay mechanism to other particles, they can pass through vast distances of matter unimpeded. Neutrinos with energies exceeding 1 EeV (10^{18} eV) present an especially interesting subject of research as they can provide insight into the most energetic accelerators of the observable universe. **U**ltra-**H**igh **E**nergy **N**eutrinos (UHEN) in this energy range have yet to be directly detected. Detecting UHEN above 1 EeV or setting new constraints on their flux is the **P**ayload for **U**ltrahigh **E**nergy **O**bservations' (PUEO) primary objective. To accomplish this, PUEO is sensitive to several channels of radio production by UHEN in Earth's atmosphere and ice sheets. Estimating this sensitivity before initiating an experiment is crucial to its success. Consistently updating and improving numerical simulations helps to create the most accurate predictions. This thesis explores developments to PUEO's simulations, as well as the implications of results from new sensitivity estimates.

1.1 Neutrino Production Mechanisms

UHEN can be produced throughout the universe by several processes which can be used to categorize cosmogenic and astrophysical neutrinos. Detection and reconstruction of these neutrinos can give insight into the location and processes by which they were produced. Cosmogenic neutrinos are produced through the interaction of propagating **U**ltra-**H**igh **E**nergy **C**osmic **R**ays (UHECR) with the **C**osmic-**M**icrowave **B**ackground(CMB). Astrophysical neutrinos are neutrinos which are produced directly by large astrophysical objects. These objects

could include pulsars, supernovae, and neutron star mergers, which produce neutrinos through hadronic and photo-hadronic processes [1].

Proton UHECR can produce cosmogenic UHEN through the **G**reisen-**Z**atsepin-**K**uzmin (GZK) process [4, 5]. The GZK process involves the production of neutrinos through proton photoproduction: when a proton cosmic ray interacts with photons of the CMB to produce mesons. These mesons can decay to gamma rays and neutrinos, with gamma rays taking the majority of the initial proton energy. However, current measurements have limited the GZK-produced UHEN flux expected on Earth, leading to development of new models. One of these models of UHEN production is through high-mass UHECR which undergo photodisintegration and generate neutrinos. Knowing the theoretical production mechanisms suggests that in conjunction with UHECR measurements, reconstructed cosmogenic UHEN could be used to help identify sources and constrain the flux of UHECR.

PUEO expects to have a leading sensitivity to astrophysical sources that produce short, large bursts of neutrinos (transient sources) such as supernovae and flaring blazars [1]. This specialization in transient fluxes is due to PUEO's instantaneous aperture to UHEN, removing the need for long-run statistics to declare a detection.

1.2 Radio Detection Techniques

As UHEN pass through Earth they produce radio through their interactions with matter and with Earth's magnetic field. The two primary emission channels that PUEO is sensitive to are Askaryan emission (dominating in in-ice particle showers) and geomagnetic emission (dominating in extensive air showers). These types of emission compose the several different

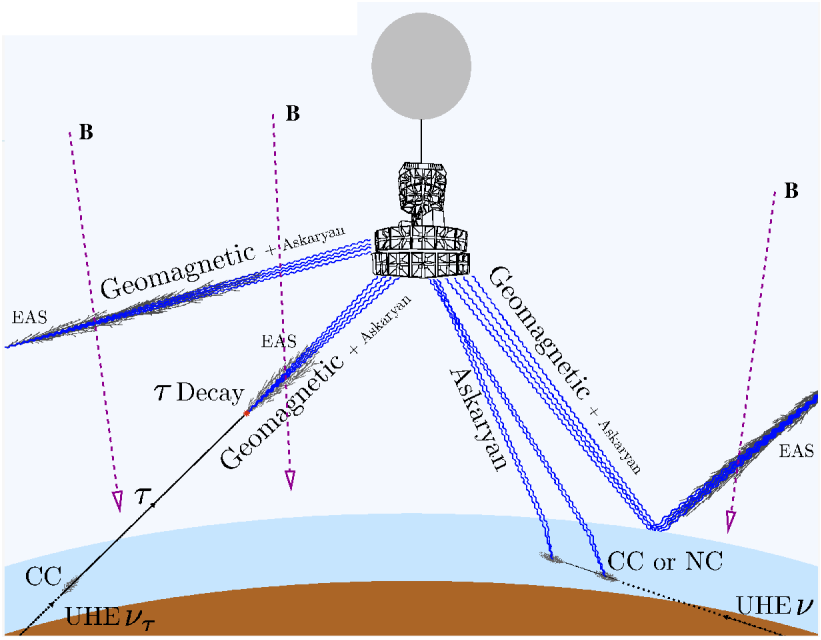

Figure 1: Diagram of all event channels that PUEO is sensitive to. Note that several channels contain multiple types of emission. Geomagnetic emission is the predominant component of Tau EAS, however a small amount of Askaryan emission is also produced during these events. [1]

types of events PUEO expects to be sensitive to shown in Figure 1. PUEO benefits from its high-altitude location above Antarctica to substantially increase its visible volume of air and ice, resulting in an increase in expected sensitivity.

In-Ice Askaryan Emission

When UHEN pass through a dense dielectric like ice, they can initiate a particle shower that creates a negative charge excess on the shower front [6]. This effect is similar in mechanism and production to Cherenkov radiation, in which UHEN must be moving greater than the phase velocity of light in ice. The excess charge is primarily created through charged current or neutral current interactions of UHEN with nucleons. A UHEN interacting with the nucleons of the dense dielectric could produce leptons with similar momentum direction to the original UHEN through

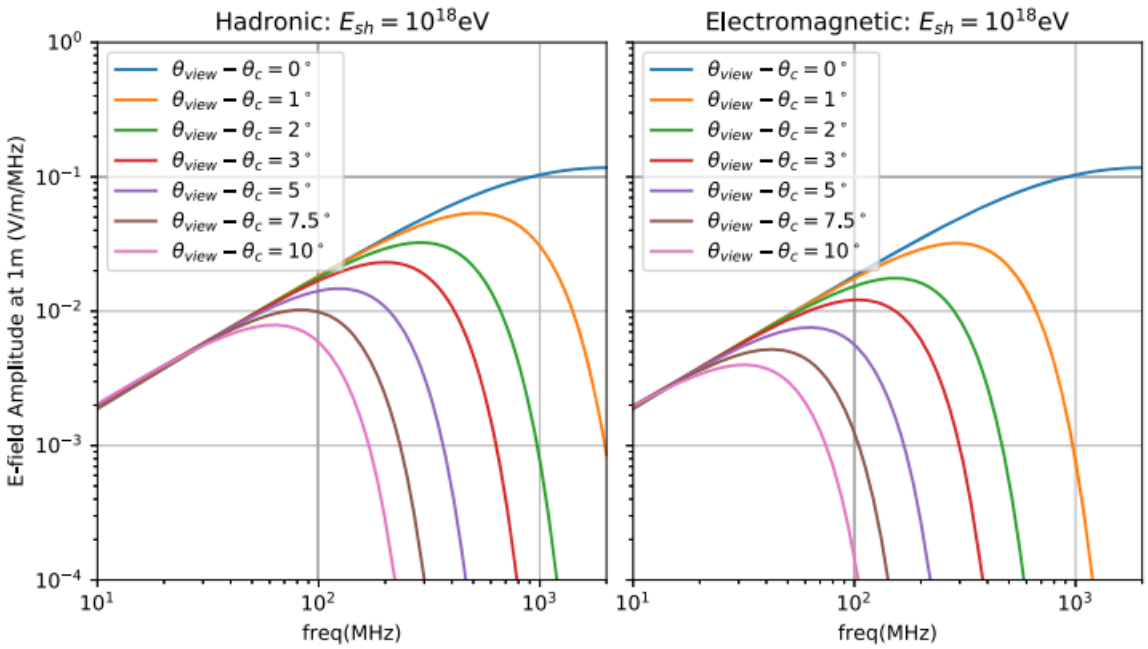

Figure 2: Frequency spectrum of Askaryan emission for varying shower types and view angles from the propagation axis. On-cone events (view angle = 0), have the largest power with high frequency components dominating. [2]

these interactions. These leptons then continue to initiate an electromagnetic or hadronic shower which emits coherent radiation in the radio spectrum through a Cherenkov-like effect.

For the strongest and most impulsive events, Askaryan emission scales approximately linearly with increasing frequency, with a detectable signal across approximately 1 GHz of the spectrum as seen in Figure 2. This is why having broadband antennas is very important to PUEO; sensitivity to a larger phase space of the signal allows one to decrease the trigger thresholds needed. An antenna with a broader frequency response will be able to transmit more power for a signal with a large standard deviation like Askaryan radiation.

Geomagnetic Emission in Air Showers

Geomagnetic emission has been well understood in the field of UHECR detection, as cosmic rays are known to generate this type of emission. However, UHEN can produce this radiation via

a similar mechanism. An **E**xtensive **A**ir **S**hower (EAS) developing in Earth's atmosphere can liberate electrons and positrons from the molecules in the air. These electrons and positrons separate due to Earth's magnetic field and create a strongly radiating, time-varying dipole across the shower axis. UHEN generate these EAS through a multi-step process that begins with a tau neutrino passing through Earth.

Once a tau neutrino passes through Earth, it can undergo a charged current interaction that converts it to a tau lepton within Earth's crust. If it has sufficient energy to exit it will pass through Earth's crust into the atmosphere. Due to tau's short lifetime and decay length on the order of 10^2 km, many will decay while still in the atmosphere, generating an upgoing EAS that gives off geomagnetic radiation as described above. Geomagnetic emission from upgoing tau's can be distinguished from geomagnetic emission from downward cosmic rays due to the phase shift seen when downward showers reflect off of Earth's surface. Unlike Askaryan radiation, geomagnetic emission for upgoing taus peaks in the 25-75 MHz range and decreases with increasing frequency as seen in Figure 3.

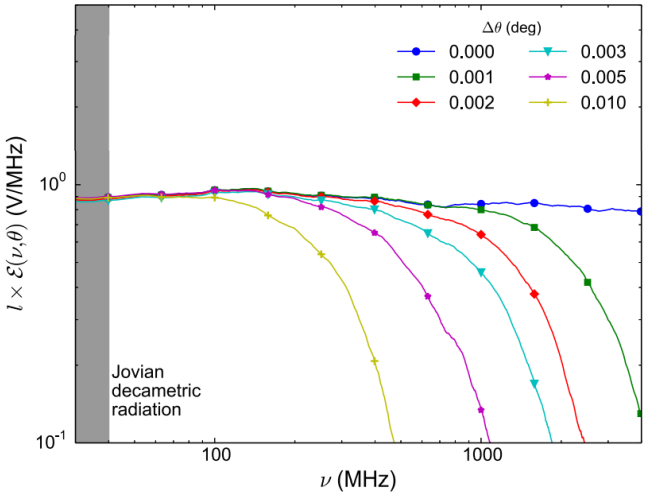

Figure 3: Frequency spectrum of a simulated air shower, for varying view angles from the propagation axis. On-cone events (view angle = 0), have the largest power with high frequency components dominating. [3]

Upgoing tau air showers are especially interesting for PUEO as they provide unique information about their generation. The polarization of their emission corresponds with the direction of Earth's magnetic field at that location, allowing easier reconstruction. In addition, the emission cone of geomagnetic air showers is typically smaller than that of Askaryan emission, providing a narrower pointing resolution on the order of 1°.

1.3 Prior ANITA Limits and Anomalous Events

Through the four flights of PUEO's predecessor mission ANITA, between 2006 and 2016, new limits on diffuse UHEN flux were set in addition to several UHECR air shower detections. These flights have paved the way for PUEO's development and design improvements from the previous ANITA flights. ANITA was able to provide the best constraints of UHEN flux for energies $10^{19.5}$ – 10^{21} eV [1]. The first detection of UHECR from EAS was made through ANITA I's flight above Antarctica. Most cosmic ray events detected by ANITA were those reflected off the surface of the ice, since cosmic rays are down-going as opposed to neutrinos which could pass through the Earth.

In addition to cosmic ray detections, there were several anomalous events observed by ANITA that resemble EAS but do not fit the characteristics of a downward going UHECR. These events were primarily horizontally polarized and originated from a range of angles below ANITA's horizontal. However, they did not demonstrate the polarity shift that reflected UHECR showers must have. Five of these events are candidates for direct, above-horizon cosmic rays that had elevation angles of -4.3°, -3.4°, -2.3°, -5.5°, and -3.6°. However, two of these anomalous events came from very steep angles below ANITA's horizontal; -27.4° and -36.7°**.** These elevation angles are not what is expected for upwards going tau neutrinos, as their cross section

does not suggest significant decay rates after exiting Earth's crust at these angles. This opens the potential for new physics explanations to describe these events, including supersymmetry and dark sector models.

These anomalous events and multiple signals in the EAS channel have motivated the inclusion of an additional antenna array to PUEO. A **L**ow **F**requency (LF) array operating at 50 – 300 MHz is an addition to PUEO's design that will have an order of magnitude higher sensitivity to UHECR and UHEN EAS. This instrument, in addition to an improved trigger, will increase PUEO's sensitivity to this channel with the goal of providing more confidence in the origin of these anomalous events.

2

PUEO Mission and Design

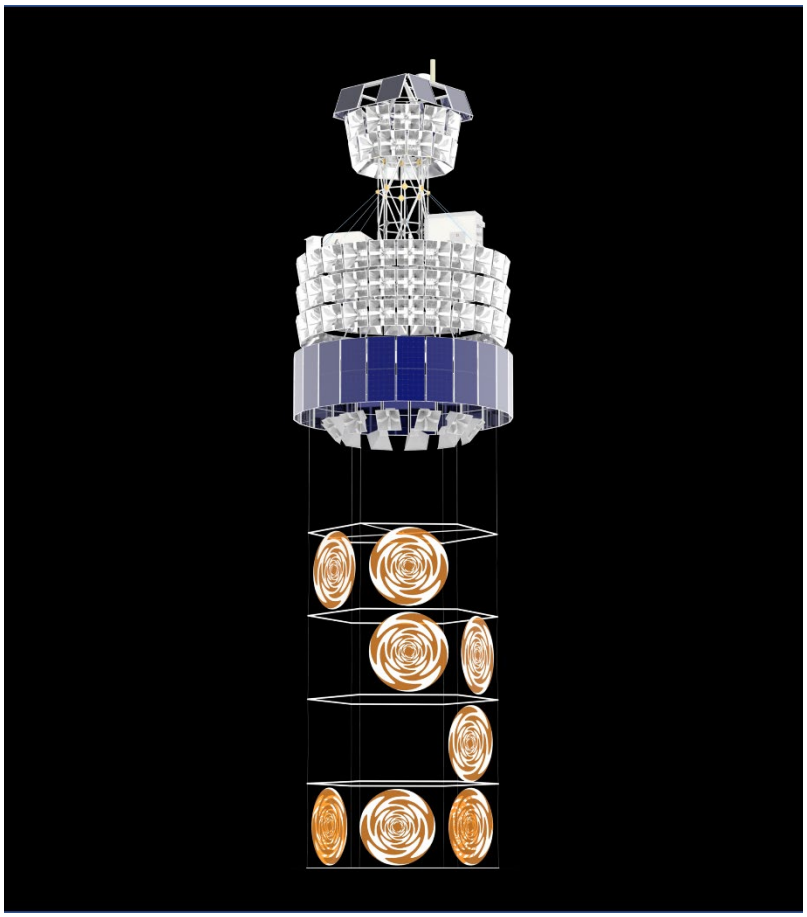

Figure 4: Rendering of PUEO's payload containing the MI and LF Instrument. [1]

The PUEO experiment is a collection of radio antenna detector arrays that will be balloon-borne in an elliptical path above Antarctica. A series of several interconnected components are necessary to effectively detect an event, reconstruct its origin, and characterize its type. These components are intended to respond to the incident electric field of a geomagnetic or Askaryan emission event, amplify its signal to be louder than background noise, and save enough information to investigate characteristics of the event.

2.1 Overview of Subsystems

The two primary systems within the PUEO experiment are the **M**ain **I**nstrument (MI) and **L**ow **F**requency (LF) Instrument. These two detector arrays contain mostly parallel versions of subsystems that serve similar purposes between the two detectors, with some differences.

The first interaction points of the payload with its external environment are the antennas. These have a known response to external electric fields over different frequencies and directions called the antenna gain. Knowing the gain and the relative positions of all the antennas can be used to reconstruct the directions of the incoming signal.

After the antennas have responded to an electric field signal, this information travels through a **R**adio **F**requency (RF) signal chain as a varying voltage. The RF chain is a collection of amplifiers, filters, and other signal-processing electronics that attempt to increase the strength of the signal without increasing background noise. Noise is introduced to the detectors through many different sources. Man made sources like satellites create noise at well-defined frequencies that notch filters are good at decreasing. However, broadband thermal noise is present through the surroundings like Antarctica's ice sheets, galactic RF noise, in addition to the operation of all PUEO's electronics which create plenty of RF noise.

This voltage pulse is then passed through a digitizer and sent to the trigger and DAQ system. One of the most significant performance enhancements of PUEO over its predecessor ANITA is the use of a Phased Array Trigger. The Phased Array Trigger attempts to raise the **S**ignal to **N**oise **R**atio (SNR) by summing the input waveforms over all antenna channels. An

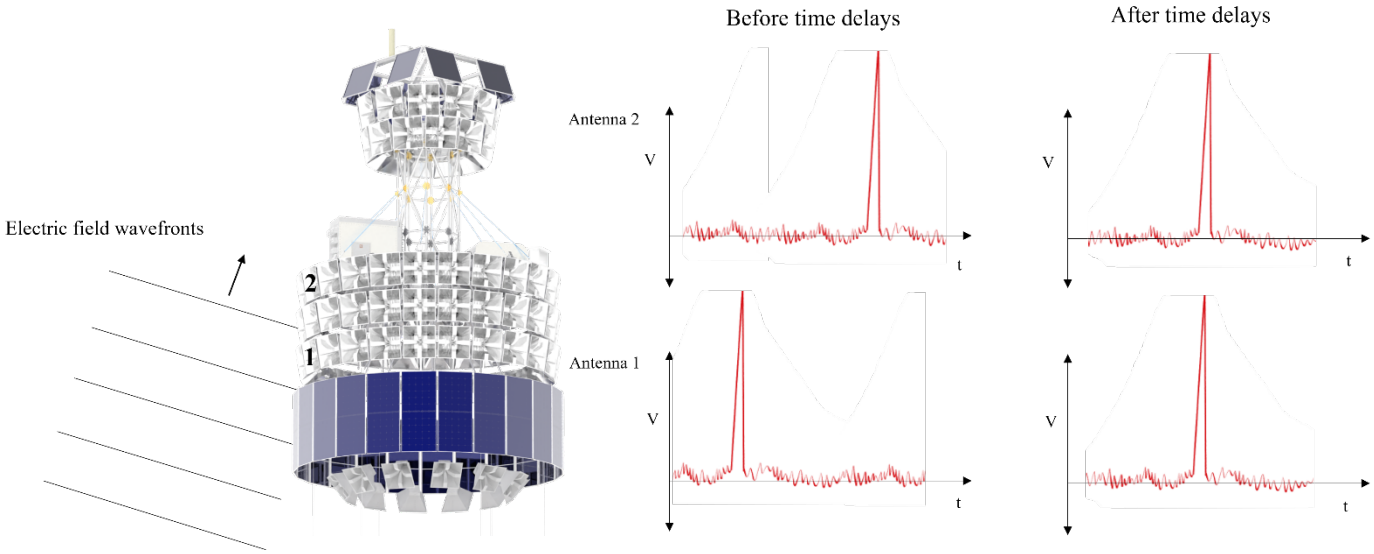

Figure 5: Diagram of an arriving electric field pulse and the effect of time delays on the recorded waveforms. V refers to Voltage and t refers to time. Plane waves are assumed for emission origins whose distance to payload is much greater than the distance between antennas.

incoming electric field for an emission event will have peak voltages at different times between all the antennas, since it has to travel between them as illustrated in Figure 5. To align the peak voltages in time, the waveforms are shifted according to time delays that correspond to some incident electric field angle. These shifted waveforms are then added together in an attempt to increase the signal magnitude by a factor of N (number of antennas). Since thermal noise is uncorrelated, its shifted sum will not be coherent and will not see as large an increase in magnitude as the signal, which results in an average SNR increase of $\sqrt{N}$. This process is repeated over many possible incident electric field angles; if the largest SNR of these possible angles is greater than some predetermined threshold, a positive trigger is declared. The reason many possible incident angles are tested is because it is too computationally intensive for the detector to instantaneously reconstruct an incident angle for every signal window, since most of the time the detector will just be reading noise. Rather, it is better to assume a range of possible angles to calculate time delays and see for which angle would a coherent sum increase the SNR.

2.2 Main Instrument

PUEO's Main Instrument consists of a collection of 108 dual-polarized horn antennas, an RF signal chain, **S**ampling **U**nits for **RF** (SURF), **T**rigger **U**nits for **RF** (TURF), and a DAQ system for storing triggered events. The horn antennas are designed for a broadband response, having a peak gain in the 300 – 1200 MHz band. Since they are dual-polarized, there are 2 output channels for each antenna that correspond to vertical and horizontal electric field polarizations. They are arranged in 5 rings extending vertically down from the payload, where each ring has antennas arranged radially from the payload. Each antenna contributes to one of 24 phi sectors, which are a grouping of antennas that share a similar azimuthal directivity as shown in Figure 6. The lowest ring of the MI antennas called the nadirs will be deployed post-launch and are canted downwards at a -40° angle from the horizontal, as opposed to -10° for the upper 4 ring antennas. The nadirs serve to increase the sensitivity to EAS events and any potential similar candidates to the ANITA anomalous events.

The MI's RF chain includes low and high pass filters at 300 and 1200 MHz respectively. This bandwidth is chosen to avoid man-made noise from satellites which occurs predominately

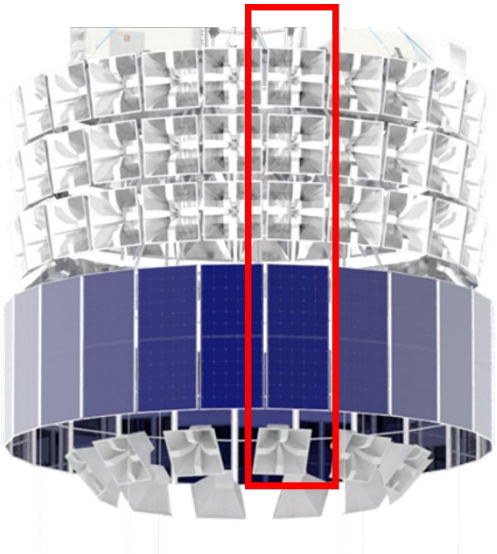

Figure 6: One of 24 phi sectors outlined in red.

in the 200-300 MHz range. A cascade of low-noise amplifiers and other signal processing units results in an amplification of the received antenna signal by ~60 dB. The SURF boards are 16-channel processing units that digitize the signal coming from the RF chain. Each SURF handles the response from antennas making up rings 1-4 within 2 adjacent phi sectors; a total of 8 dual polarization antennas. The dual polarization results in 16 channels entering each SURF. The digitized signals then exit the SURF and are processed by the TURFs for the phased-array trigger system.

The phased-array trigger system consists of 3 separate processes. The Level 1 (L1) Trigger performs the beamforming (applying time delays and summing channels) to the channels belonging to the 2 adjacent phi sectors for each SURF. This beamforming is performed 60 times corresponding to different possible incident electric field azimuth and elevation angles. Each beamformed waveform is called a beam, where all beams span a range of 30° in azimuth and 45° in elevation angle. A squared power sum is performed on each beam and a trigger is declared if it passes a predetermined threshold. Events that passed the L1 Trigger are sent to the L2 trigger, which performs the same beamforming process on a collection of 2 adjacent SURFs; a total of 4 adjacent phi sectors. This doubles the spanned range in azimuth to 60° and serves to narrow down the collected list of events to those that were strong enough to be seen in many more antennas. Events that pass the L2 trigger are sent to the L3 trigger, which performs final cuts based on event polarization and other factors. The TURF saves the antenna data to disk only for events which passed all 3 trigger levels. With a set trigger rate of 100 Hz, the flight computer ends up processing 50 MB/s of data.

Figure 7: Half-scale model of a LF Sinuous antenna

Figure 8: Half-scale model of deployable LF frame

2.3 Low Frequency Instrument

The Low Frequency Instrument parallels many of the same components of the Main Instrument. The LF consists of 8 nylon-ripstop fabric antennas, its own RF chain, SURF and TURF boards, and a DAQ system. The antennas are fabric-based to make them easily loaded into the payload to reduce PUEO's pre-deployment size. Each 2 x 2m nylon-ripstop sheet will be coated with a nickel, copper, silver alloy that will act as the receiving antenna. Each alloy coating takes the form of a sinuous pattern seen in Figure 7 with 4 independent pieces that will allow discrimination between vertical and horizontal polarizations. The antennas are arranged in a hexagonal carbon fiber ring structure supported by nylon rope as displayed in Figure 8. Similarly to the MI, there are 4 vertical levels of antenna rings, which will be suspended from the center of

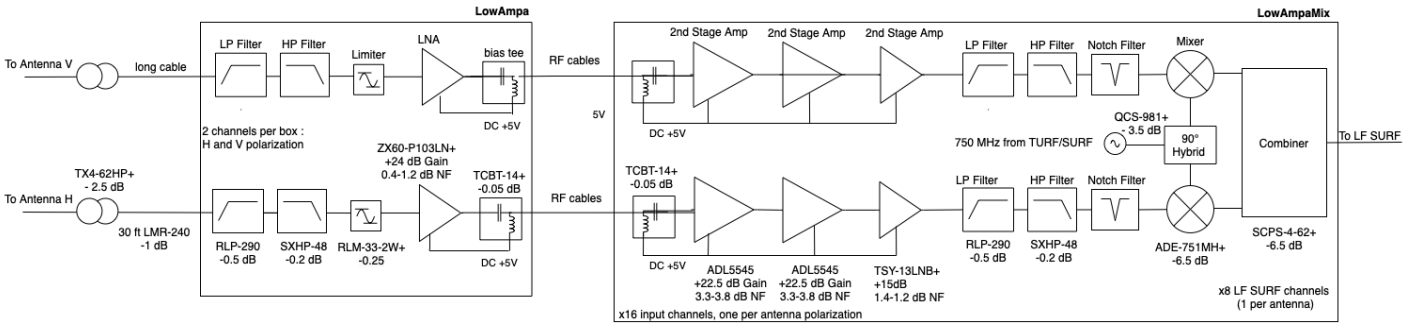

Figure 9: RF signal chain configuration for LF Instrument

the payload after deployment. These antennas have a peak responsivity in the 50 – 300 MHz band, serving to increase PUEO's sensitivity to EAS events which are expected to have larger power in this low frequency band.

The LF's RF chain has high and low pass filters at 50 and 300 MHz respectively. It includes several notch filters at specific known satellite frequencies to reduce anthropogenic sources of noise. A simulation study determined that using RF cables as opposed to RF over fiber caused no significant decrease in detector sensitivity, which resulted in the current RF chain configuration choice shown in Figure 9. All 8 of the dual-polarization LF sinuous antennas are fed into a single 16 channel SURF board that performs the same digitization as described for the MI. A full trigger system is still under development for the LF instrument, however it is planned to operate under similar principles as the MI. An L1 trigger for the LF instrument would utilize a coincidence scheme between all antennas, while an L2 trigger would perform beamforming for 5 of the LF antennas through the same process as described in Section 2.2.

3

Simulation Techniques and Components

Simulation tools are required to make predictions for various components of PUEO's detectors in addition to estimating its overall sensitivity. Before physical models of a detector are constructed, simulating the detector response allows one to consider design changes and prototyping without wasting expensive materials and fabrication time. For particle detectors like PUEO, there are two tasks to complete within a simulation package: simulating the particles that could be detected, and simulating the response of the detector to these particles. These steps occur in two primary components called Monte-Carlo Generators and Detector Response. Monte-Carlo Generators randomly sample certain parameters that define the particles' propagation and interactions. They generate large quantities of these events which are then sent to the detector response component. Detector response components contain all the necessary information about the detector to determine whether it would have triggered on individual events. This information could include the physical geometry of the detector, the gain of the antennas, the trigger, and the signal chain among others. The final output of these simulations is some quantity that describes the fraction of events which were detected of those that could have been detected.

3.1 Monte Carlo Generation in TAPIOCA

The **Ta**u **Poi**nt S**o**urce **Ca**lculator (TAPIOCA) is a simulation package that contains a Monte-Carlo generator for upgoing tau air showers as well as a simplified description of the antennas for the MI and LF instruments. TAPIOCA's Monte-Carlo generator iterates through a multi-step

process that simulates the entire course of a neutrino's eventual geomagnetic emission. This process involves creating a random sample of neutrino events in an Earth coordinate system, assigning random decay lengths to each event, approximating the electric field generated during the EAS, and propagating this electric field through the atmosphere to the location of the detector.

Before sampling begins, there are several adjustable parameters chosen that determine the event properties. Neutrino initial energy within the range of 10^{17} – 10^{21} eV, range of elevation angles below PUEO's horizontal, and number of events to be thrown are several of these parameters. Once these parameters are chosen, TAPIOCA generates events during iteration through each elevation angle.

Generation begins with determining a point on the surface of the Earth that is located at the given elevation angle from PUEO. Once this point is found, a segment is laterally projected onto the surface of the Earth that corresponds to a small displacement of the elevation angle as shown in Figure 10. This small elevation angle displacement is typically set to 3°, twice the size

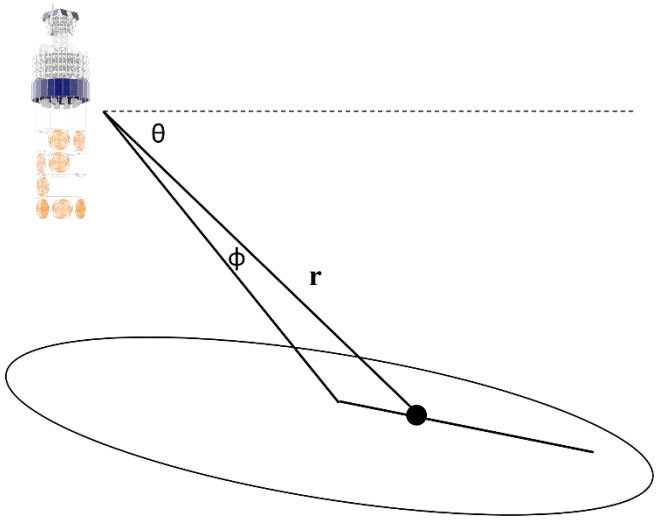

Figure 10: Segment generation on surface of Earth. Elevation angle θ determines "center point", with central axis vector **r** pointing from detector to this point. Max view angle ϕ sets width of segment.

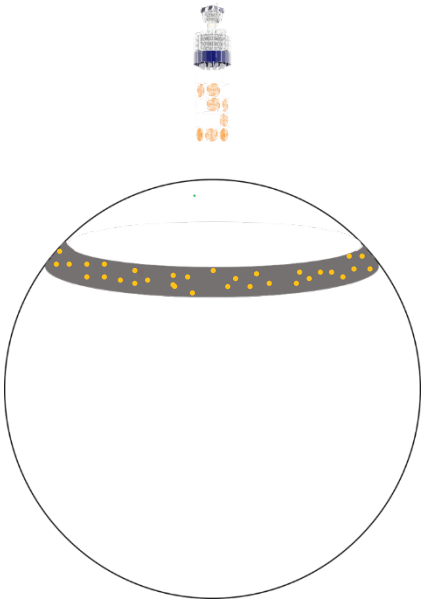

Figure 11: Final spherical segment after rotation about phi. Yellow dots indicate sampled tau lepton exit locations.

of the Cherenkov angle in air, to capture most of the signal which is strongest on the Cherenkov cone shown in Figure 3. Assuming azimuthal symmetry, this segment is rotated about phi to generate a spherical segment as shown in Figure 11.

Points are uniformly sampled on this spherical segment which serve to represent the exit location of candidate tau leptons. Each of these points is assigned a velocity vector parallel to the central axis vector **r**, because a point source flux is assumed. Based on the angle between the velocity vector and the tangent plane to that point on the sphere (emergence angle), the probability for the tau lepton to exit the Earth's crust is assigned.

These events are then each assigned an exponentially sampled random decay length based on their energy, typically on the order of 1km. The decay point in the atmosphere is found

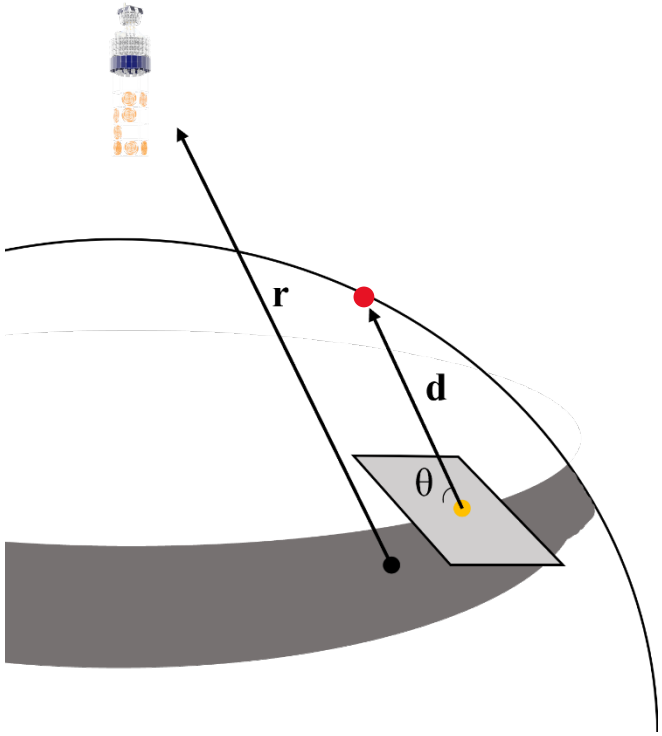

Figure 12: Decay vector of one trial tau lepton. Black dot indicates a center point as shown in Figure 10, with central axis vector **r** pointing to the detector. Decay vector **d** is parallel to **r** and has magnitude equal to the decay length. θ denotes the emergence angle of the tau from the tangent plane to the surface of the earth. The yellow dot is the location of the exit point on the surface, while the red dot is the location of the decay point in the atmosphere.

for these events based on the velocity vector and the decay length as shown in Figure 12. It is at this decay point that the electric field from an EAS can be determined.

3.2 Neutrino Propagation and Radio Production

Finding the electric field caused by an EAS from a decaying tau lepton is a lengthy and computationally intensive process. Current methods involve modeling the electric field for every particle involved in the shower and summing them over many kilometers which can take days. It is because of this that many Monte-Carlo air shower simulations will typically use a separate tool to simulate several EAS one time with many different parameters, and then interpolate over these results for future simulations.

For PUEO a simulation tool called ZHArIES is utilized that uses the ZHS formalism for numerically approximating the electric field generated during an EAS. ZHArIES was ran over an array of parameters such as the decay point's zenith angle, altitude, energy, and view angle to the detector. A **L**ook **U**p **T**able (LUT) was generated for these events, over which TAPIOCA interpolates based on the individual parameters for each TAPIOCA event. This results in a much quicker method to determine the electric field at the detector that doesn't sacrifice too much accuracy. This is achievable by utilizing the fact that generated electric fields scale inversely with propagation distance, and linearly with energy. Interpolating over multiple parameters can more accurately apply this approximated scaling.

3.3 Detector Response

After the interpolation of the electric field emission, the next step is to calculate the response of the detector to this electric field. This is necessary to determine whether PUEO would have triggered on this event or if it would have passed unnoticed. The detector response component consists of detailed descriptions of the physical systems of PUEO, in addition to the calculations involved in the trigger.

For TAPIOCA, geometry of the MI and the LF instrument are included as well as the gain patterns on each antenna. These allow calculation of the electric field as seen in the antenna, which will vary according to the direction it arrives at the antenna relative to the antenna gain. After the antenna response is determined, TAPIOCA and other detector response simulations send this waveform through the entire signal chain of the detector. This signal chain includes electronics such as amplifiers, notch filters, low/high pass filters, and various other components that are intended to increase the strength of the signal in the frequency range anticipated before sending it to the trigger.

In addition to modeling the electric field detected by PUEO, it is necessary to model the electromagnetic noise expected to be recorded by the instruments. Electromagnetic fields are present everywhere; in PUEO's visible frequency band noise can be seen from the surrounding galaxy, Antarctica's ice sheets, satellites, in addition to interior electronics. Galactic and thermal noise from ice sheets have been well documented and can be added to simulations from existing data. Noise introduced from RF signal chains have been measured in lab and recorded as a power spectrum. These noises are all summed and added to the signal in simulation before being sent to the trigger.

For the LF instrument in TAPIOCA, a coherent sum trigger is implemented that allows for amplification of the signal through synchronizing the delays between the antennas. Since the electric field arrives at the detector at some angle, it will peak in each antenna at different times. Calculating the delay between these pulses, and adjusting the signal so that the pulses occur at the same time, allows one to coherently add the waveforms to amplify the signal and improve the Signal to Noise Ratio (SNR). This amplification serves to increase the chances of triggering on true signals. A simple SNR threshold value is used to determine if the detector triggered on this signal. If the detector had a larger SNR than the threshold, the event is marked to have triggered the detector. This information is later used to calculate the expected effective area.

3.4 Effective Area and Sensitivity Calculations

The end goal of this simulation is to estimate PUEO's point source sensitivity to upgoing tau air showers. Point source sensitivity refers to a detector's ability to detect emission from one point in the sky. This differs from diffuse sensitivity which assumes that same emission could come from a broad range of angles. Sensitivity is a broad term that can be expressed in different units depending on the goals of the detector. For most high energy astrophysics purposes, sensitivity refers to the number of particles needed to claim a detection per unit area, per unit energy, over a given period of time. This means that detectors with smaller values of sensitivity require fewer passing particles to make a detection for a given area, energy, and time period.

One method to estimate a detector's sensitivity is to calculate its effective area. Effective area is the area over which the instrument is sensitive to neutrinos weighted by the fraction of events that the detector is able to trigger on and their exit location on the surface of the earth. Effective area has units of km^2 as each event contributes a certain differential area dependent on

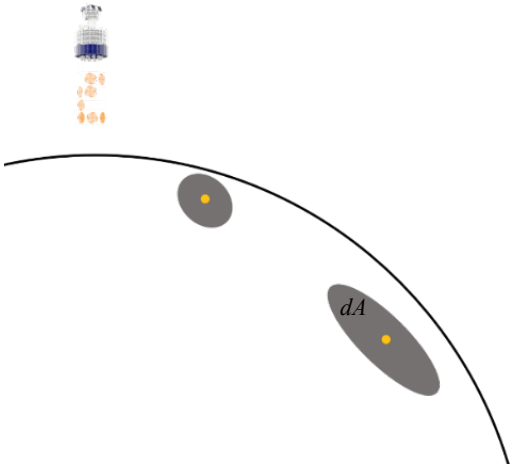

Figure 13: Differential areas contributed by different event exit locations. Points at steeper elevation angles will contribute smaller differential area.

their exit location from the surface. Events closer to the horizon contribute a higher differential area than those directly below the payload as shown in Figure 13. If the detector were able to trigger on every event that is thrown, the effective area would be equal to the total surface area PUEO can see. Effective area is used as a metric because it provides an idea of how a better trigger efficiency will lead to an effectively larger detector, as PUEO's "detector" is essentially Earth's ice sheets and atmosphere.

TAPIOCA is able to estimate the effective area with the trigger results of the process described in this chapter. A simple calculation is used to make this estimation. As mentioned in section 3.1, the probability for the particle to exit is saved during the emergence angle calculation. Additionally, the probability for the particle to decay is saved as a result of the randomly sampled exponential decay length. The probability for the particle to trigger the

detector is saved as either 0 or 1 dependent on the results of the trigger as described in section 3.3. These parameters are combined to calculate the effective area by summing over each event,

$$Area_{eff} = Area_{geo} \sum_{i} D_i P_i^{trig} P_i^{decay} P_i^{exit} \quad (1)$$

where $Area_{geo}$ is the total geometric area on the surface of the Earth seen by PUEO, D_i is the dot product of the particles' exit location with the central axis vector **r** (to encode its area contribution), and the P's are the trigger, decay, and exit probabilities. Effective Area is inversely proportional to point source fluence sensitivity, while a diffuse flux sensitivity can be found by integrating the effective area over all zenith and azimuthal angles, and then taking the inverse.

4

Integration of Taus into Upgraded Detector Response

For most of the collaboration's history, PUEO and its predecessor ANITA have used several simulation packages to estimate the detectors' sensitivity and reconstruction abilities. TAPIOCA, as described in Chapter 3, has been used with a simplistic description of the triggers and antennas to make predictions about PUEO's response to upgoing tau air showers. pueoSim is another simulation package that contains much more detailed descriptions of PUEO's trigger architecture, RF signal chain response, geometry, and flight path. However, pueoSim has only been interfaced with a Monte-Carlo generator for Askaryan emission events. The goal of this study has been to integrate TAPIOCA's upgoing tau Monte-Carlo generator with the more expansive detector response package pueoSim to achieve up-to-date estimates of PUEO's sensitivity to taus. Several constraints involving storage capacity and language-specific data types have guided the design of the interface between these two packages. Additionally, it was discovered that external modifications to TAPIOCA's outputted electric field were necessary to be properly received by pueoSim's signal processing scripts.

4.1 Motivation and Constraints

Interfacing external Monte-Carlo generators for taus and cosmic rays into pueoSim has been a significant research interest of the PUEO collaboration. When PUEO was first proposed, tau estimates were made using a simplified description of the MI trigger and the LF antennas, as they had not been fully designed yet. As design and testing of these components have been completed, they have been reproduced in pueoSim to provide more accurate estimates of

PUEO's response to Askaryan events. Exporting generated tau events into pueoSim will provide the most accurate predictions of PUEO's tau response to date.

The largest difficulty in constructing this interface is that pueoSim is written in C++ while TAPIOCA is written in Python, creating no straightforward method to call one package from another. Several methods were considered in linking the two packages including saving data to disk and using a C++/Python wrapper. Ultimately, a direct piping structure was decided as it provided the simplest means of execution.

A direct interface that called both packages consecutively was necessary as storing the electric field data of every tau event on disk would be impractical. Originally TAPIOCA used the frequency domain representation of the incoming electric field to calculate each detectors' antenna response and signal chain amplification. The frequency domain of the electric field was stored in 25 frequency bins spanning the entire bandwidth of the MI and LF instruments. However, it was found that this representation lacked the resolution needed for pueoSim's trigger, so a time domain representation with 1024 samples was chosen. Each tau event is represented as an array of 1024, 64-bit floats. To achieve the necessary statistics for a given elevation angle ~10^5 events need to be generated simultaneously, which quickly exceed a TB of disk storage as multiple elevation angles are iterated through. This motivated the development of a serialization and piping method that only temporarily stores tau electric fields in RAM to transfer to pueoSim.

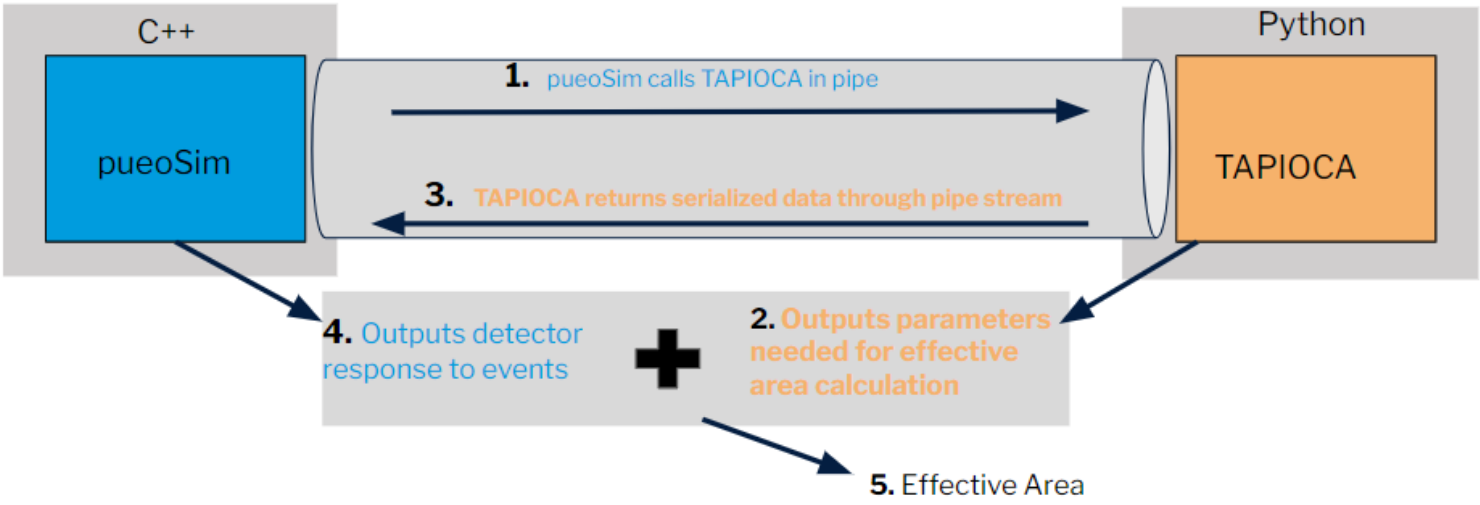

Figure 14: Diagram of data flow through package pipe structure. Outputted parameters by TAPIOCA are those from Equation 1.

4.2 Serialization and Piping Structure

Through the use of the pipe structure shown in Figure 14, the entire process of calculating effective area can be run through one driver script. This begins in a script within pueoSim, which calls TAPIOCA in a pipe. It manually passes several arguments to TAPIOCA that dictate the properties of the Monte-Carlo generation as described in section 3.1. TAPIOCA generates the specified number of events and propagates their electric field to the location of the detector. At this point, the electric field is serialized into bytes, and then encoded into a string of hex characters. Encoding the bytes into hex allows TAPIOCA to output these strings to the stream back through the pipe, ready for pueoSim to continue processing.

pueoSim receives these hex strings by reading the stream through the pipe. It then decodes the hex back into bytes and populates double arrays with the reconstructed electric field time domain data. These electric fields are passed through pueoSim's detector response, which includes the antenna gain, signal chain, and multi-level triggers. The result of the trigger for each

instrument is saved to disk, as well as the parameters from Equation 1 in section 3.4 which can be combined to calculate the effective area as demonstrated in Figure 14. This process is repeated over several elevation angles to capture the full scope of PUEO's sensitivity.

4.3 pueoSim Buffer and Resampling

During the integration of TAPIOCA events to pueoSim, it was discovered that across multiple energies pueoSim's effective area to tau events varied rapidly with elevation angle as seen in Figure 15. This non-uniform variation in effective area appeared to be non-physical behavior, as variations on the order of 10^2 km^2 do not match the initial predictions given by TAPIOCA. This led to the realization that pueoSim's noise was only being generated for 1024 samples, while external generators like TAPIOCA were migrating over events with > 2000 samples. This caused pueoSim to add artificial values when adding noise to samples greater than the 1024 range.

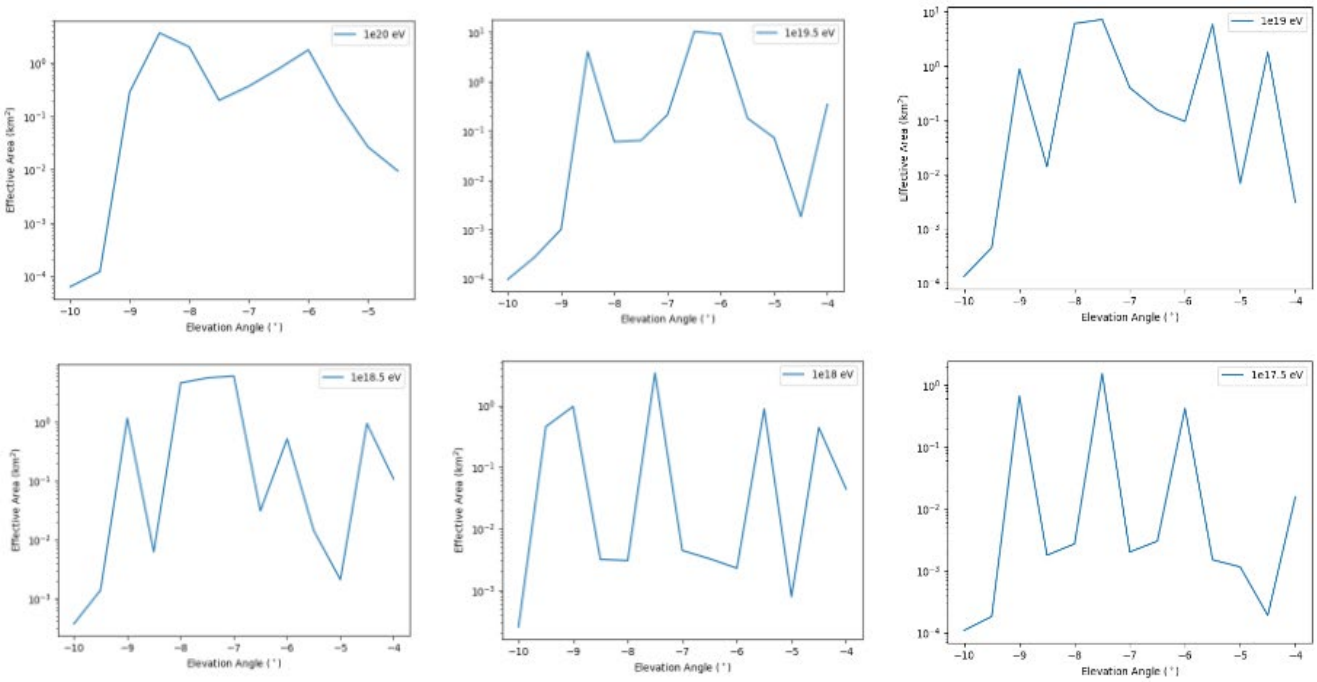

Figure 15: Artificial variations in pueoSim MI's effective area to taus. Each plot is a different initial neutrino energy.

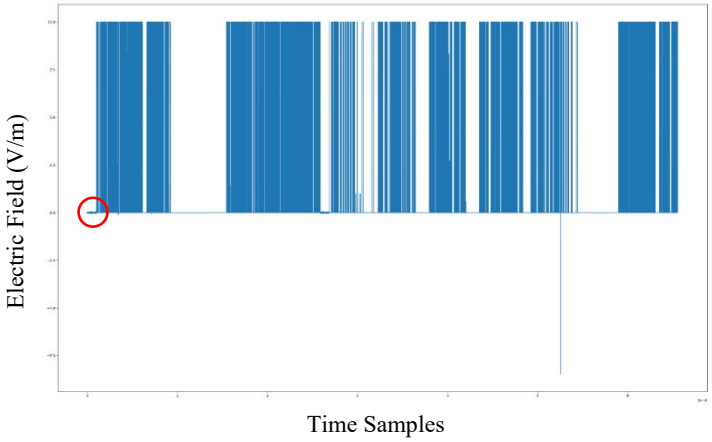

Figure 16: Electric Field waveform with NaN spikes obscuring the signal. Actual pulse shown within red circle.

When indexing outside the bounds of a defined array, C++ will draw values from random memory addresses in RAM. Occasionally, these values may be NaNs, which many languages will interpret as infinitely large values. These NaNs were being added as noise to electric field waveforms that exceeded 1024 samples, causing pueoSim to incorrectly trigger. Figure 16 shows a rough example of how NaN values are added past 1024 samples and cause the waveform to be artificially large.

A possible solution to this issue is to expand pueoSim's buffer length past 1024 samples, to fit denser sampling rates of external generators. However, this would require additional hardware changes as the sampling rate of PUEO's detectors is a physical property of the SURFs. To fit pueoSim's sampling rate, resampling was performed on each tau event before being migrated. Resampling is a process that converts a signal sampled at one rate to a different sampling rate, while preserving the power in the frequency spectrum. Depending on whether the sampling rate is being increased (upsampling) or decreased (downsampling), interpolation may be needed. Tau events were originally sampled at 2 GSa/s while pueoSim's sampling rate is 2.7

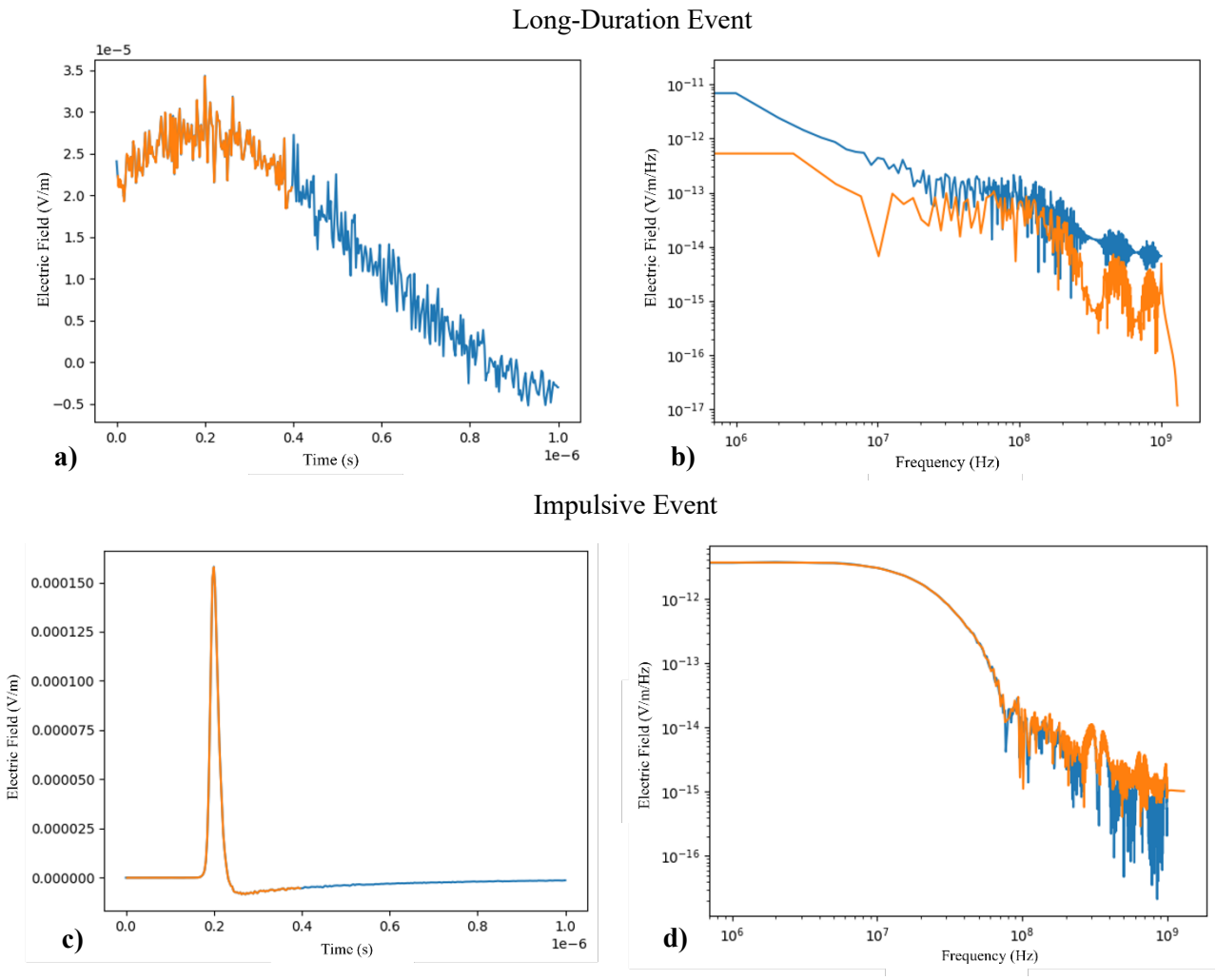

Figure 17: The time domain and frequency domain representations of two different events, where blue is the original signal before resampling and orange is after resampling. **a)** and **b)** show a long duration signal while **c)** and **d)** show an impulsive signal.

GSa/s, meaning more samples needed to be added to fit pueoSim's sampling rate density. This is illustrated in Figure 17, which shows the resampled signal compared to the original output of TAPIOCA for two different types of events. Although the new resampled signals have a higher sampling rate, the total time window for pueoSim is cut to 1024 samples, or ~400ns. For impulsive signals this changes very little. However, for long-duration signals like Figure 17a, shortening the window results in a loss of power across the band, as some of the non-zero signal is lost. The implications of this windowing on detector sensitivity are discussed in Chapter 5.

5

Broadband Observations of Taus in PUEO

The pipe structure integration described in chapter 4 allowed updated estimates of PUEO's sensitivity to upgoing tau air shower events. Through this interface, new predictions for PUEO's Main Instrument (MI) were created. However, the unique nature of air shower signals led to the discovery of a potential buffer length issue in the pueoSim's processing of external electric fields. For long-pulse duration events, pueoSim artificially magnifies its **S**ignal to **N**oise **R**atio (SNR) and increases the likelihood for a false trigger to occur. This manifests itself as a larger predicted effective area, caused by pueoSim's instruments accepting a larger span of view angles and pulse widths. Depending on PUEO's primary science objectives and the complexity of necessary adjustments, a new sampling window could be chosen to increase its sensitivity to the air shower channel.

5.1 MI Effective Area

Using Equation 1 from Section 3.4, the pueoSim's effective area to taus can be calculated with the exact same parameters as generated by TAPIOCA's Monte-Carlo. Substitution of the P^{trig} variable to distinguish trigger decisions between pueoSim and TAPIOCA's detectors is what produces the different effective area curves. Using this method, the effective area for pueoSim's MI to taus is shown in Figure 18. Unlike the previous estimates shown in Figure 15, these are within the same order of magnitude as prior estimates and have more physical validity. The increased variability of the effective area seen at lower energies is due to the greater impact of statistics at these scales. As the neutrino energy decreases, the average strength of the electric

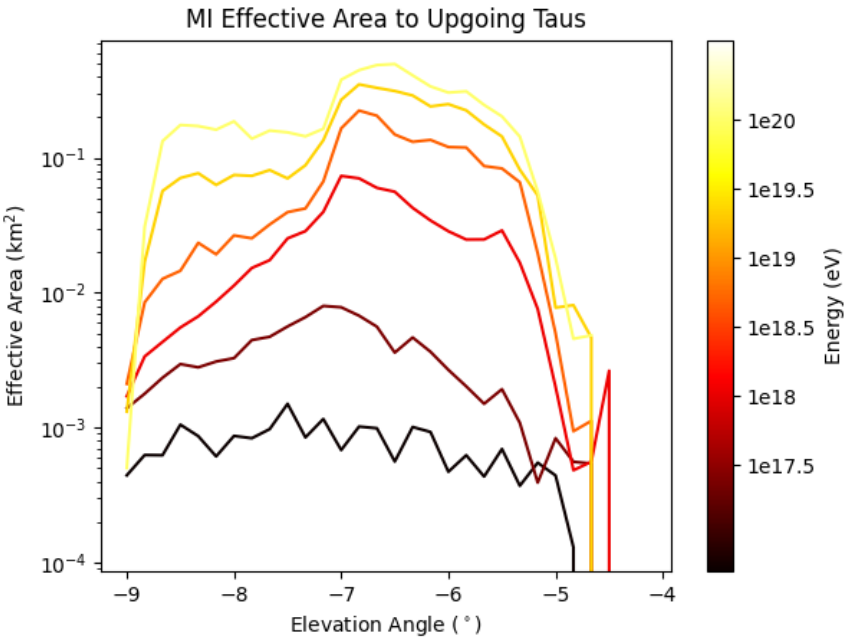

Figure 18: Effective area of pueoSim's MI to upgoing tau air showers. Shown for a range of elevation angles and initial neutrino energies.

field for generated events also decreases as it is proportional to the energy deposited in the shower. Even if a low energy run threw the same number of events as a high energy run, less events would pass the trigger at lower energies. This results in wider variability for the effective area, as each passing event has more significance when there are less total passing events.

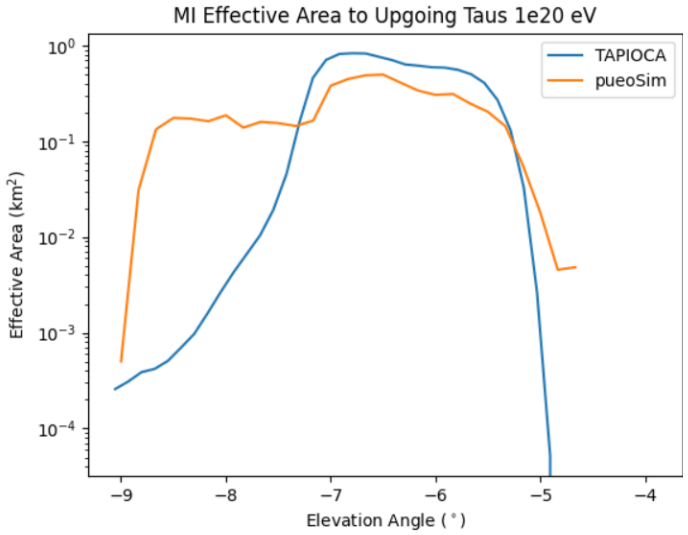

Figure 19: MI Effective area curve at an initial neutrino energy of 10^{20} eV, shown for the two simulation packages.

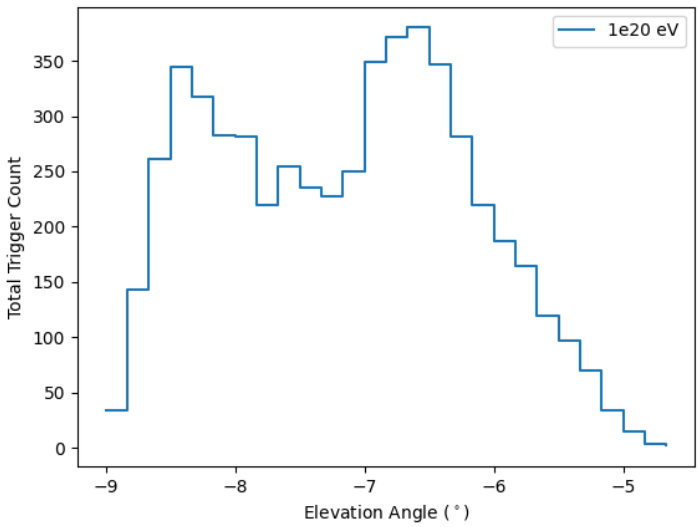

Figure 20: Raw, unweighted trigger counts for pueoSim's MI at 10^{20} eV.

These effective area curves differ in one significant region from the previous estimates made using TAPIOCA's detector response. Figure 19 shows the effective area curve for both packages at an initial neutrino energy of 10^{20} eV. TAPIOCA produces a more smoothly varying curve with maximum around an elevation angle of -6.5°. However, pueoSim's MI effective area curve produces a "double peak" structure, with a secondary shelf of larger effective area seen around an elevation angle of -8.5°. This structure is even more apparent when looking at unweighted triggers, shown in Figure 20. Unweighted triggers refer to the raw number of positive triggers recorded at every elevation angle. This quantity is a representation of the P^{trig} variable in Equation 1 and can be easily converted to effective area by using that same equation. In Figure 20 it is evident that there is a strong increase in the number of triggers around an elevation angle of -8.5°, causing the secondary shelf seen pueoSim's MI effective area.

5.2 Long-Pulse Signals and Response

While investigating the cause for the shelf structure, it was discovered that the signal processing systems within pueoSim's MI significantly distorted the shape of many tau electric fields. Figure 21 shows the electric field of an event that was triggered by pueoSim's MI. This event is uncharacteristically strong for a long-duration pulse. Typically, impulsive events with short pulse widths are expected to be the strongest compared to a long-duration pulse event with the same shower energy. However, this was a relatively strong long-duration event, a result of the Monte-Carlo's broad sampling of possible shower energies. As opposed to impulsive events, where pueoSim's processing has no issue, the digitized waveform shown in Figure 22 after passing through the antenna response and signal chain presents a very different pulse shape than the

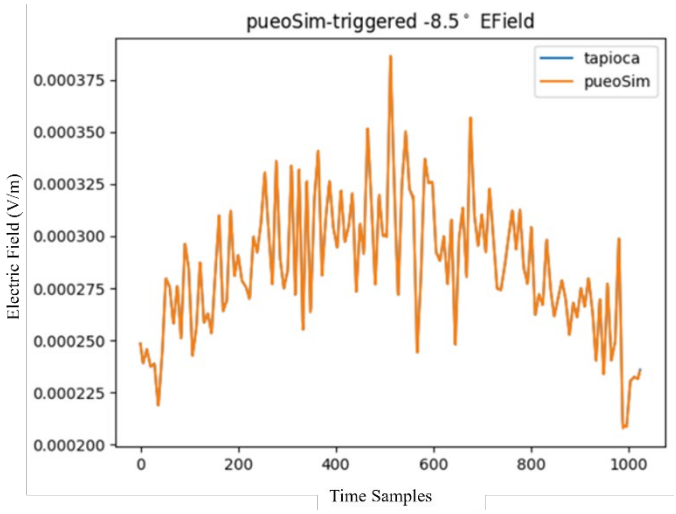

Figure 21: Electric field of a triggered long-duration pulse event at the detector. TAPIOCA and pueoSim's electric fields exactly overlap which is expected; differences between simulations should only appear after the antenna response.

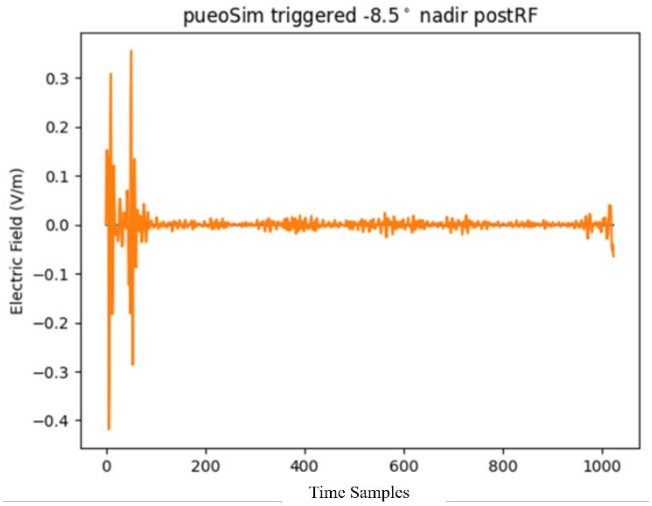

Figure 22: Digitized waveform of the electric field from Figure 21. Shown after passing through the response of a pueoSim MI nadir antenna and RF signal chain. Pulse maximum and shape does not match original electric field.

original electric field. If pueoSim's MI was working properly as it does for impulsive signals, the maximum of the pulse would still be centered in the waveform after processing. However, it consistently incorrectly processes these long-duration pulses at some point within the antenna response or the RF signal chain.

Although these long-duration signals may look unphysical or as result of a numerical artifact, they are well defined within TAPIOCA's Monte-Carlo. Investigating the origin of these pulses demonstrates what event qualities they possess. Figure 23 shows waveforms of the electric field of an upgoing tau air shower for different view angles with a fixed decay altitude and zenith angle. These waveforms demonstrate that the duration of the pulse varies smoothly with increasing view angle. The electric field at an angle 1° off the propagation axis of an air shower will appear to be impulsive and short lived, however for farther off-axis angles this pulse widens. This effect is also seen in other event properties. For a fixed view angle, fixed zenith

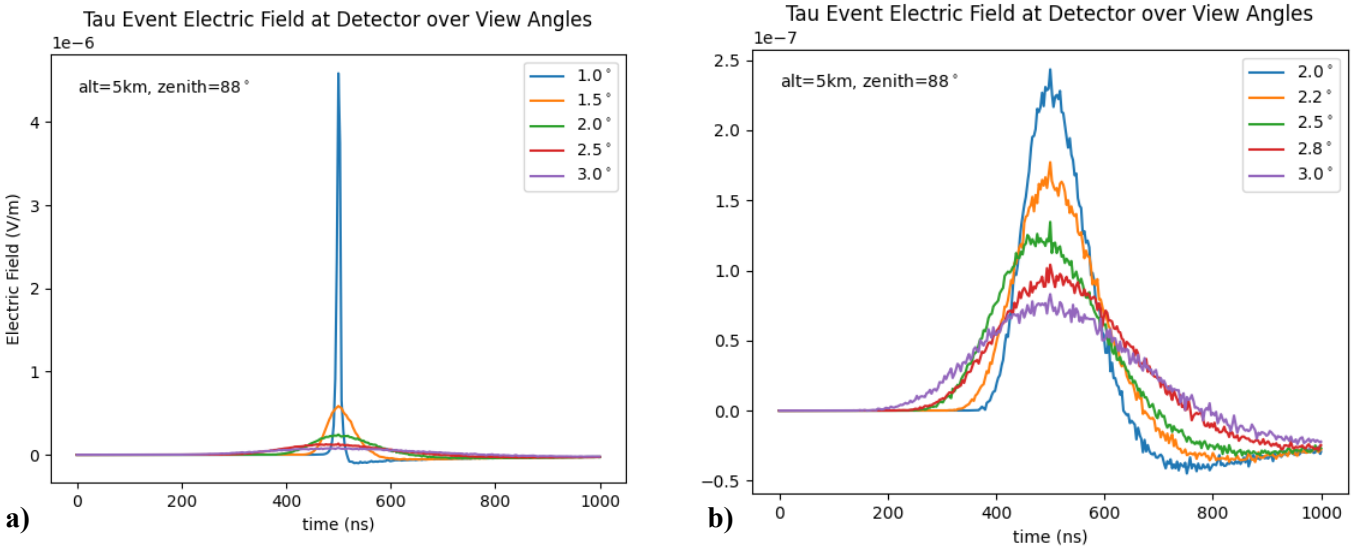

Figure 23: Electric field of a upgoing tau air shower for several view angles. Simulated at a fixed shower energy of 10^{17} eV, fixed decay altitude of 5km, and fixed zenith angle of 88°. **a)** is a coarse scan through view angles while **b)** is a fine scan through larger view angles to show variations in signal spread.

angle, and fixed shower energy, the same trend is observed as seen in Figure 24. As the decay altitude of an event is increased, the duration of the pulse also increases.

All considered, this information suggests that the long-duration pulses that are improperly processed and triggered by pueoSim are far off-cone, high altitude events whose randomly

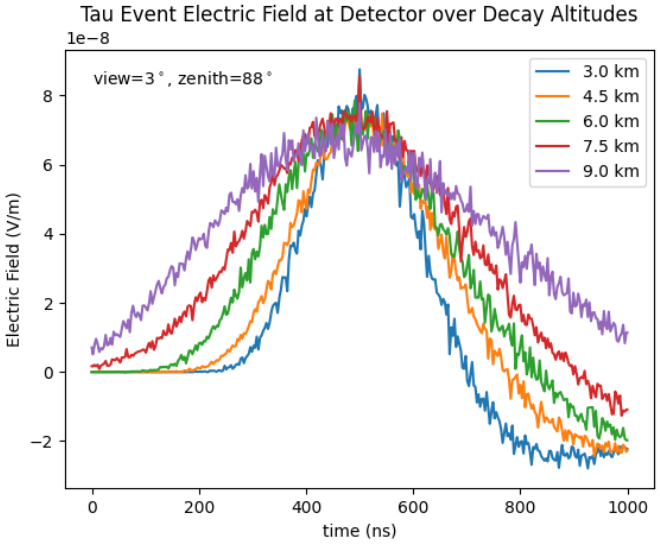

Figure 24: Electric field of a upgoing tau air shower over several decay altitudes. Simulated at a fixed shower energy of 10^{17} eV, fixed view angle of 3°, and fixed zenith angle of 88°.

sampled shower energy happened to be great enough to pass the trigger threshold. The longest of these signals have significant nonzero signal being cut off by pueoSim's ~400ns threshold.

5.3 Accepted View Angles and Pulse Widths

These long-duration pulses can be correlated with the shelfing artifact seen in Figure 19 by investigating the variation of signal length over event elevation angle. For the purposes of this paper, "pulse width" is defined as the time delay between the electric field's maximum amplitude and minimum amplitude. This serves as a measure of the duration of a signal to quantify its spread over time, as it has been seen in Section 5.2 that long-duration signals are improperly processed in pueoSim. By calculating the pulse width for each electric field, and averaging over all of TAPIOCA's randomly sampled events, there is a clear local maximum near elevation angle -8.5° as seen in Figure 25. This correlates with the spike in unweighted triggers in Figure 20. Additionally, the average view angle of these events also shows a local maximum near elevation angle -8.5°. This is expected, since Figure 23 demonstrates that pulse width and

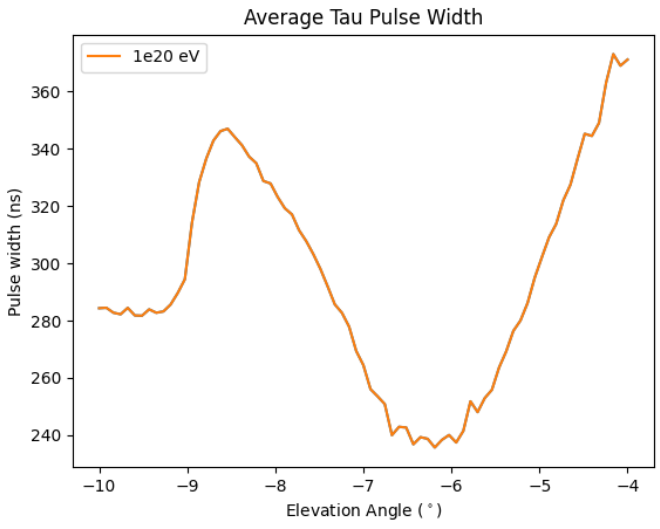

Figure 25: Average pulse width of all thrown upgoing taus. More impulsive events are seen near the horizon at -6.5°. Calculated before resampling and window cut.

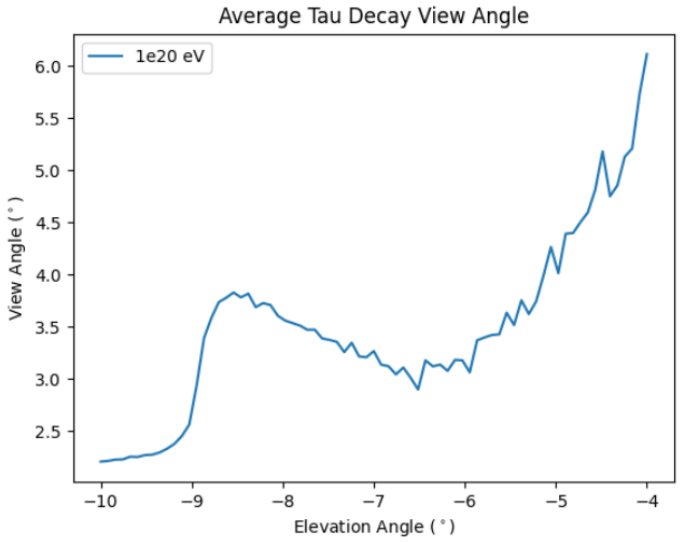

Figure 26: Average view angle of all thrown upgoing taus. More on-cone events are seen near the horizon at -6.5°.

view angle are directly proportional to each other. Nonetheless, these provide a strong implication that the false secondary shelf seen in Figure 19 is correlated with large pulse width and large view angle events.

This relationship can further be investigated by analyzing the properties of events that pueoSim triggers on compared to those that triggered TAPIOCA. A violin plot is one useful method to visualize variable distributions over certain parameters. A violin plot displays histograms of one variable across several values of a different parameter. In this instance, a violin plot displaying histograms of electric field pulse widths, over several values of elevation angle would be illuminating. In Figure 27 we can see violin plots for the pulse widths of upgoing tau air shower events. Figure 27a shows pulse width distributions for all generated events. It is evident that TAPIOCA's Monte-Carlo generates more long-duration events than impulsive events across all elevation angles at this energy range. However, an increase in impulsive events

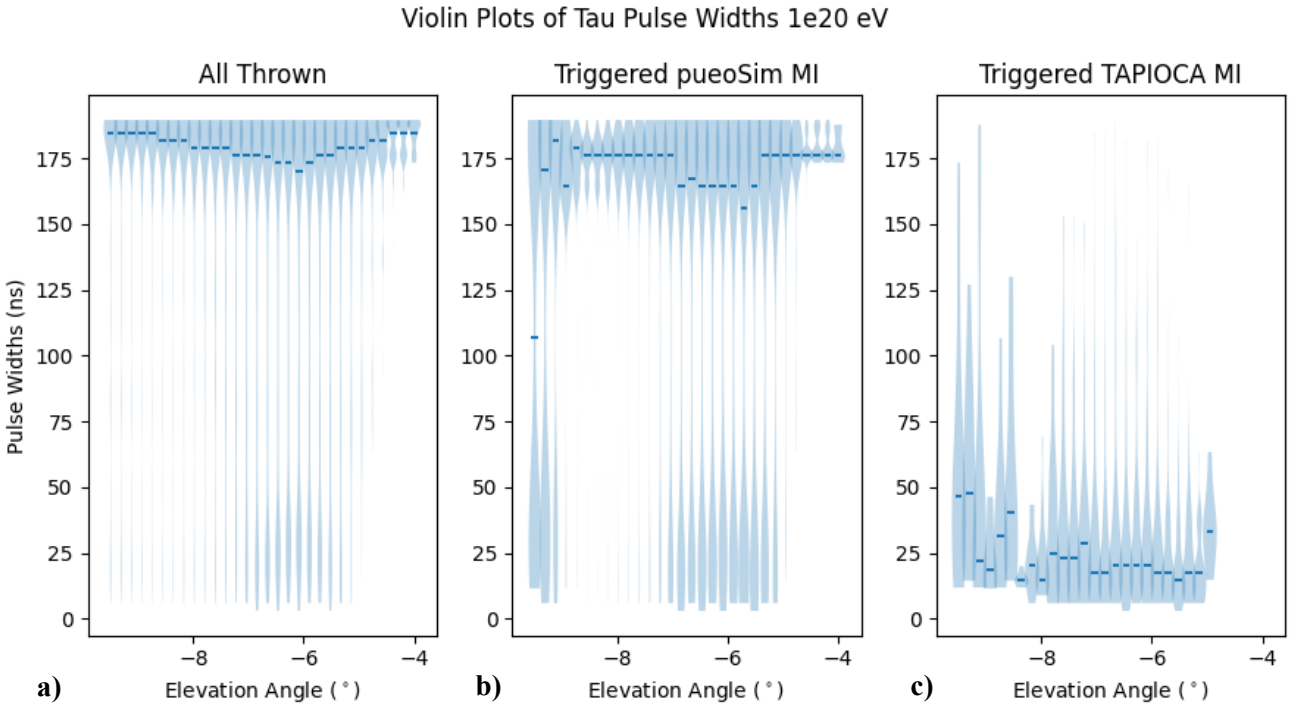

Figure 27: Violin plots for the pulse widths of upgoing tau air showers, as a function of elevation angle. Dark blue dots indicate the median of each individual histogram. Note pulse width was calculated after resampling and window cut of ~400ns, meaning maximum pulse width could only be ~200ns. **a)** is a representation of all events generated, while **b)** and **c)** are filtered to only include MI triggered events.

is seen near an elevation angle of -6.5°, evidenced by a darker shaded area in the low pulse width region in Figure 27a. If these events are filtered by only those that trigger the MI, it can be seen in Figure 27c that TAPIOCA only accepts shorter, more impulsive signals for most elevation angles. This is not the case for pueoSim's MI, which allows many more long-duration signals to pass its trigger in addition to the impulsive events as seen in Figure 27b.

Since an event's view angle and pulse width are directly proportional (as demonstrated in Figure 23), this same behavior can be observed in violin plots of tau view angles. The difference between pueoSim's and TAPIOCA's accepted events is even more drastic when comparing the view angles seen in Figures 28b and 28c. As expected, TAPICOA's accepted view angles lie very closely to the Cherenkov cone angle of ~1° for air showers. However, across all elevation angles pueoSim accepts a much broader range of view angles than TAPIOCA.

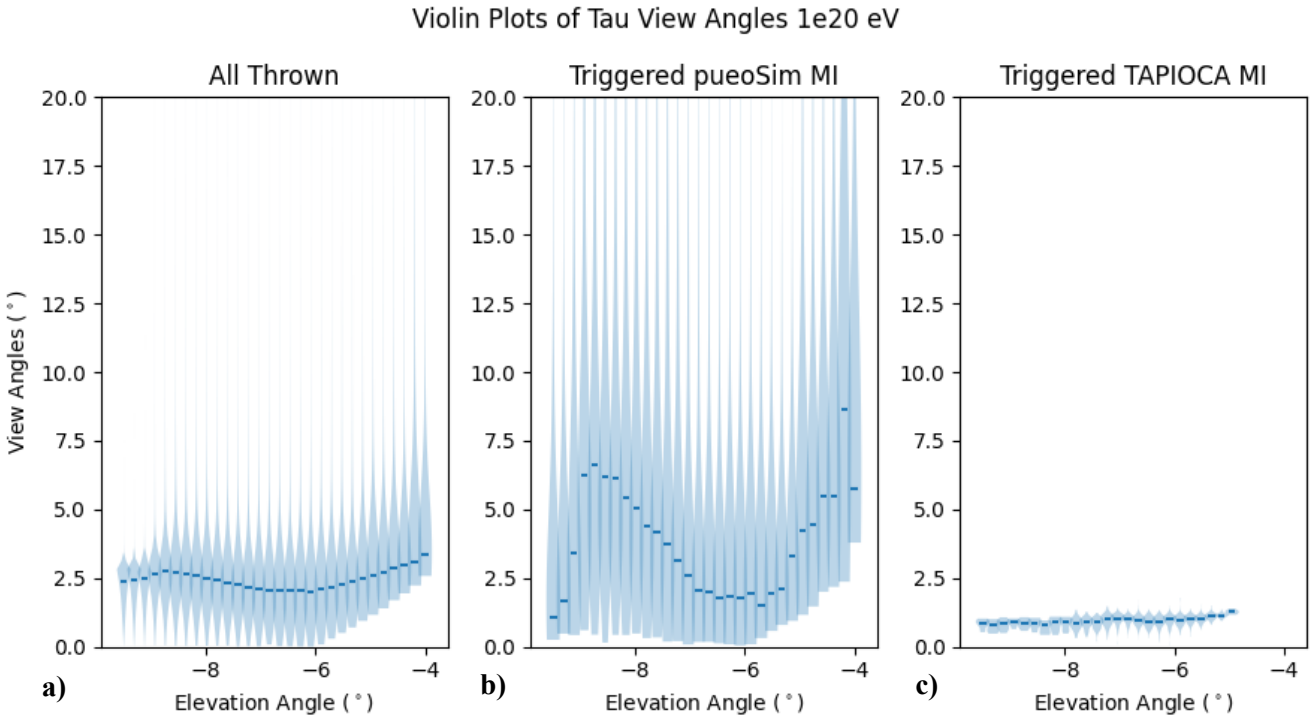

Figure 28: Violin plots for the view angles of upgoing tau air showers, as a function of elevation angle. Dark blue dots indicate the median of each individual histogram. **a)** is a representation of all events generated, while **b)** and **c)** are filtered to only include MI triggered events. Plot maximum was cut at 20° for visualization purposes, but view angles were generated up to 80°. Note that the medians of **a)** follow the same curve of means in Figure 26.

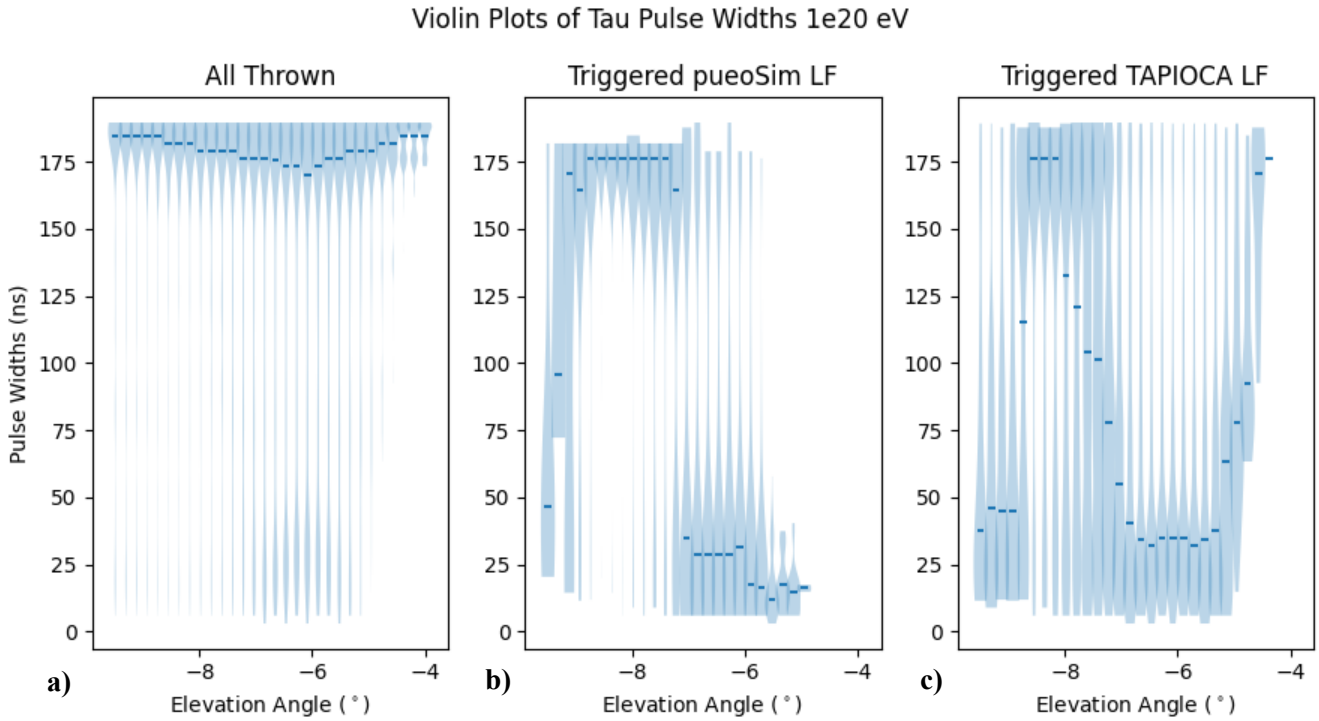

Figure 29: Violin plots for the pulse widths of upgoing tau air showers, where **b)** and **c)** are filtered to only include LF triggered events. See Figure 27 for plot descriptions.

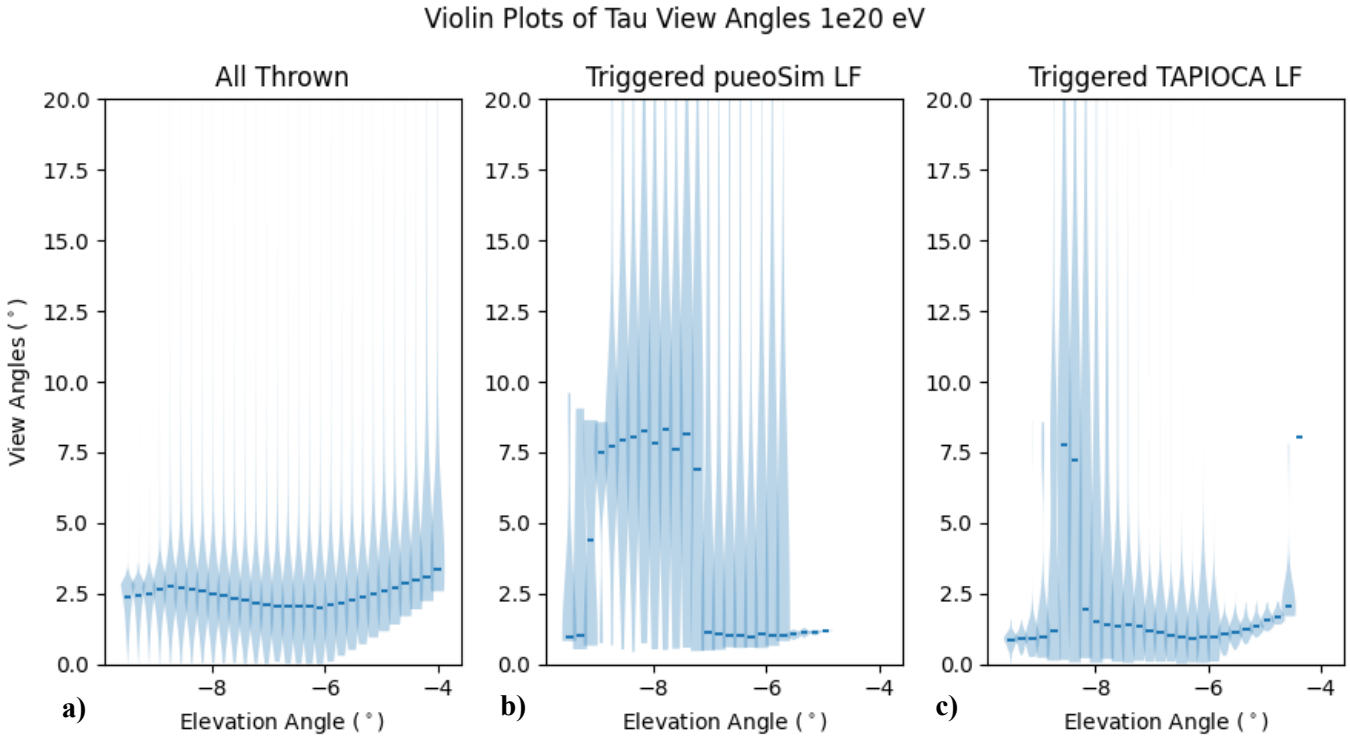

Figure 30: Violin plots for the view angles of upgoing tau air showers, where **b)** and **c)** are filtered to only include LF triggered events. See Figure 28 for plot descriptions.

Electric fields with more power in the low frequency band (such as off-cone air shower events) have longer pulse lengths since more of their signal is contributed from components with long wavelengths. Since the LF instrument is better configured to handle low frequency signals, it is anticipated that the issue with improper triggering on long-duration signals should not be as apparent in the LF instrument. This is demonstrated in violin plots for view angles and pulse widths triggered by the LF instrument. In Figure 29, the triggered pueoSim pulse widths are a closer match to TAPIOCA's triggered pulse widths than those for the MI in Figure 27. Additionally, pueoSim's LF instrument accepts a more similar range of view angles to TAPIOCA's LF instrument as seen in Figures 30b and 30c. This is not the case for pueoSim's MI, as previously mentioned above and shown in Figure 28.

5.4 SNR Magnification and Diagnostics

A useful parameter to investigate false triggers in any simulation is the SNR of the event. In most trigger schemes, the power sum threshold (described in Section 2.2) used to determine a trigger will be proportional to the SNR. Since noise will be relatively consistent throughout the duration of an experiment's run, a power sum threshold can be set based on a minimum SNR that the experimenter's decide is required to analyze the event. This results in the ability to quantify trigger thresholds in terms of SNR. To compare the strengths of individual events between the two packages, a histogram of the SNRs can be made. Note for all SNR figures in this paper, "pueoSim SNR" refers to the maximum single antenna SNR, multiplied by a factor of $\sqrt{N}$ to account for the beamforming amplification described in Section 2.2. "TAPIOCA SNR" refers to the direct beamformed SNR computed by TAPIOCA.

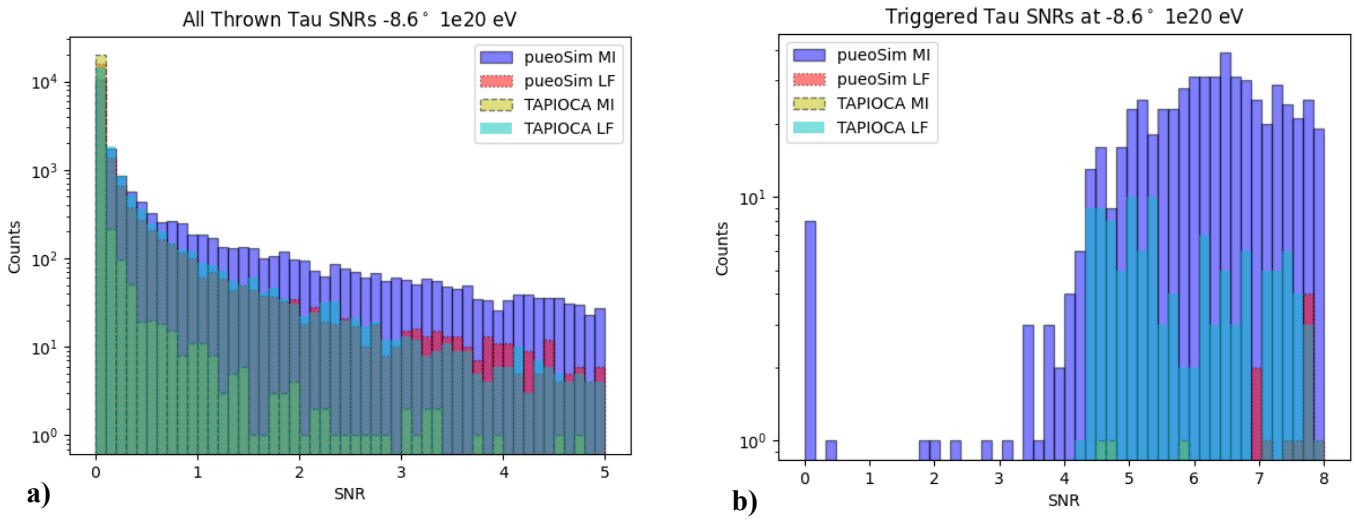

Figure 31: Histograms of SNRs produced by the detectors for events at elevation angle -8.6° and initial neutrino energy 10^{20} eV. **a)** shows all generated events while **b)** is filtered for only triggered events. Note that histogram colors will blend when overlapping, so TAPIOCA's MI histogram appears green for most of the plots.

Figure 31 shows histograms of SNRs for the 4 different simulated detectors. It can be seen in Figure 31a that pueoSim's MI dominates throughout the range of SNRs; pueoSim's MI outputs many more large SNR events than TAPIOCA's MI. However, it can also be seen that there is relatively good matching between TAPIOCA's LF instrument and pueoSim's LF instrument, correlating with results from Figures 29 and 30. Figure 31b demonstrates the effect of pueoSim MI's larger SNRS, where there are many more triggered events in that category than

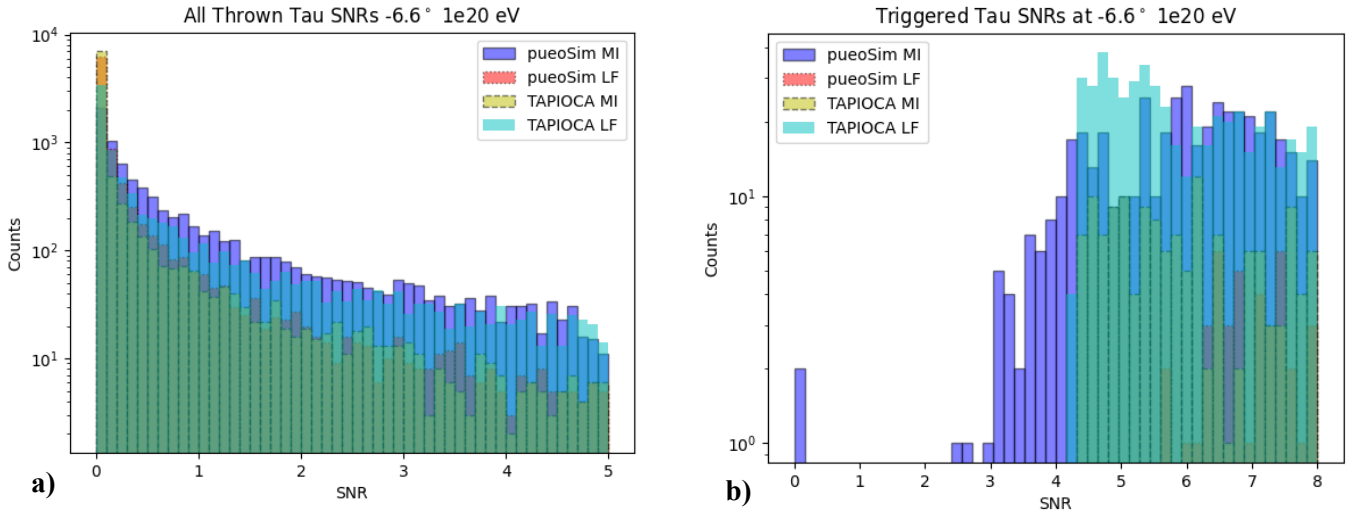

Figure 32: Histograms of SNRs produced by the detectors for events at elevation angle -6.6° and initial neutrino energy 10^{20} eV. See Figure 31 for plot descriptions.

for TAPIOCA's MI. Interestingly, TAPIOCA's LF instrument seems to have a lower SNR threshold than pueoSim's LF instrument. TAPIOCA's LF begins triggering at 4.3 SNR, however pueoSim's LF does not trigger until ~7 SNR. This difference between simulation packages, although still present, is not as severe at an elevation angle of -6.6° seen in Figure 32.

The strongest evidence for the cause behind pueoSim's artificial triggers can be seen by relating pueoSim's increase in SNR to the pulse width of the event. Figure 33a shows a simple correlation plot comparing the SNR produced by pueoSim's MI as a function of the SNR in TAPIOCA's MI on an event-by-event basis. Evidently, as the vast majority of events fall above the red y=x line where the two SNRs would be equal, pueoSim is producing larger SNRs than TAPIOCA for the same event. Additionally, it appears a larger magnification of the SNR is occurring for TAPIOCA SNRs near 0. This can be explained by analyzing the ratio between pueoSim SNRs and TAPIOCA SNRs as a function of the event's electric field pulse width in

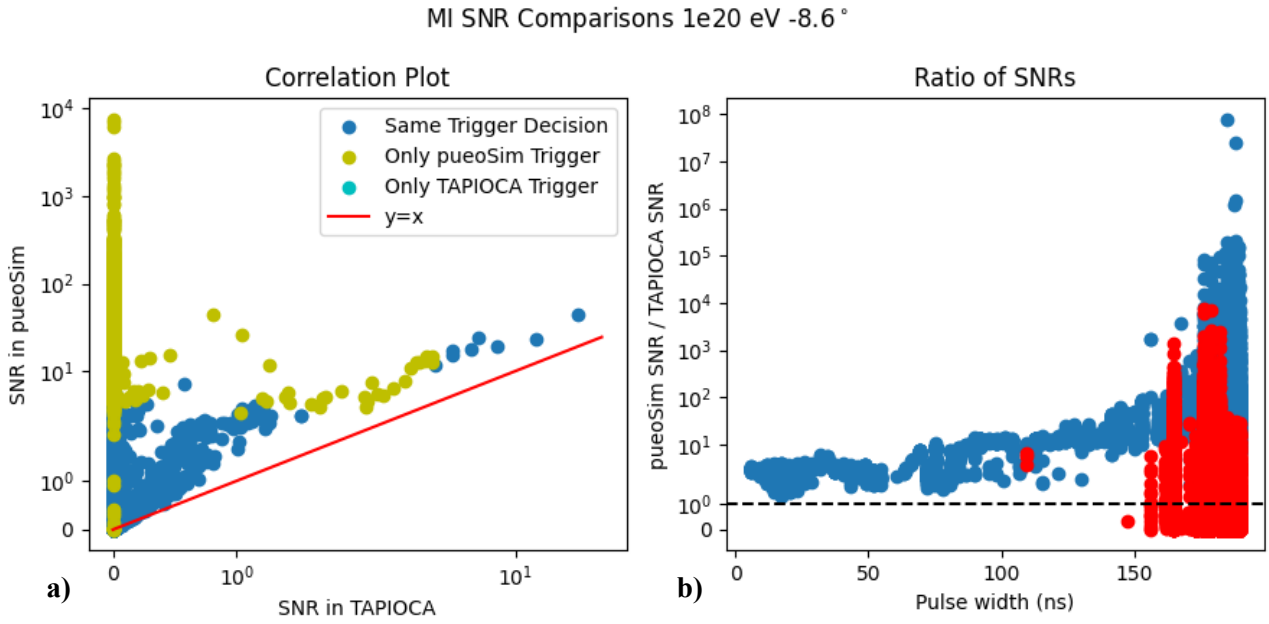

Figure 33: Comparisons of MI SNRs for events at elevation angle -8.6° and initial neutrino energy 10^{20} eV. **a)** shows pueoSim's SNR for a given TAPIOCA SNR, where yellow dots indicate events that only triggered pueoSim, while blue dots indicate both simulations had the same trigger decision of either no trigger or a positive trigger. There were 0 events that only triggered TAPIOCA. Blue dots in **b)** show the ratio of SNRs between pueoSim and TAPIOCA, while red dots show the raw SNR in pueoSim for events that had a 0 value of SNR in TAPIOCA.

Figure 33b. The majority of ratios fall above the dashed y=1 line where the two SNRs would be equal and seem to exponentially increase with increasing pulse width. Additionally, even for events that produced a 0 value of SNR in TAPIOCA, pueoSim still produced a nonzero SNR.

It is no coincidence that SNRs of 0 value in TAPIOCA cluster around longer pulse widths seen in Figure 33b. Long-duration events are expected to have less power than their impulsive counterparts (illustrated in Figure 23b), meaning long-duration events are more likely to produce low SNRs. This behavior precisely explains the sharp peak of large pueoSim SNRs seen in the low TAPIOCA SNR region of Figure 33a. Those larger pueoSim SNRs are exactly the long pulse width, low TAPIOCA SNR events being magnified in Figure 33b. This behavior is less severe but still apparent in the MI SNR comparisons at -6.7° of Figure 34, where more events follow the y=x line of 34a, and the ratio distribution of 34b is slightly flatter than 33b. This is again due to the presence of more impulsive events near -6.7° as shown in Section 5.3.

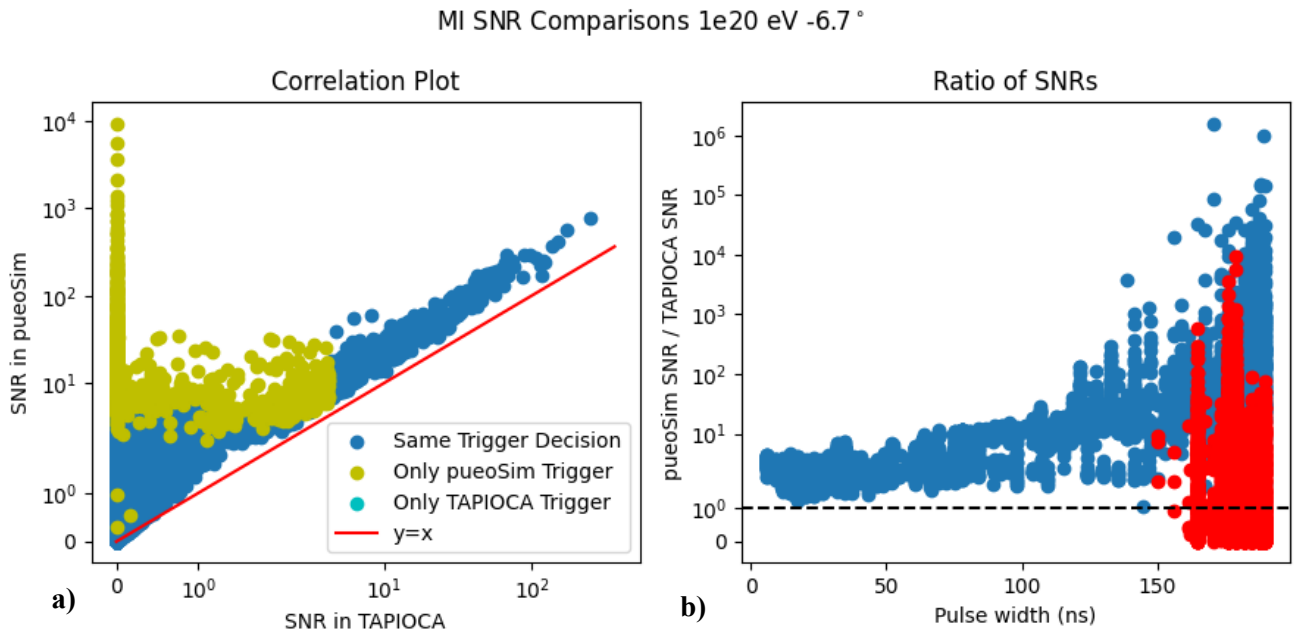

Figure 34: Comparisons of MI SNRs for events at elevation angle -6.7° and initial neutrino energy 10^{20} eV. See Figure 33 for plot descriptions.

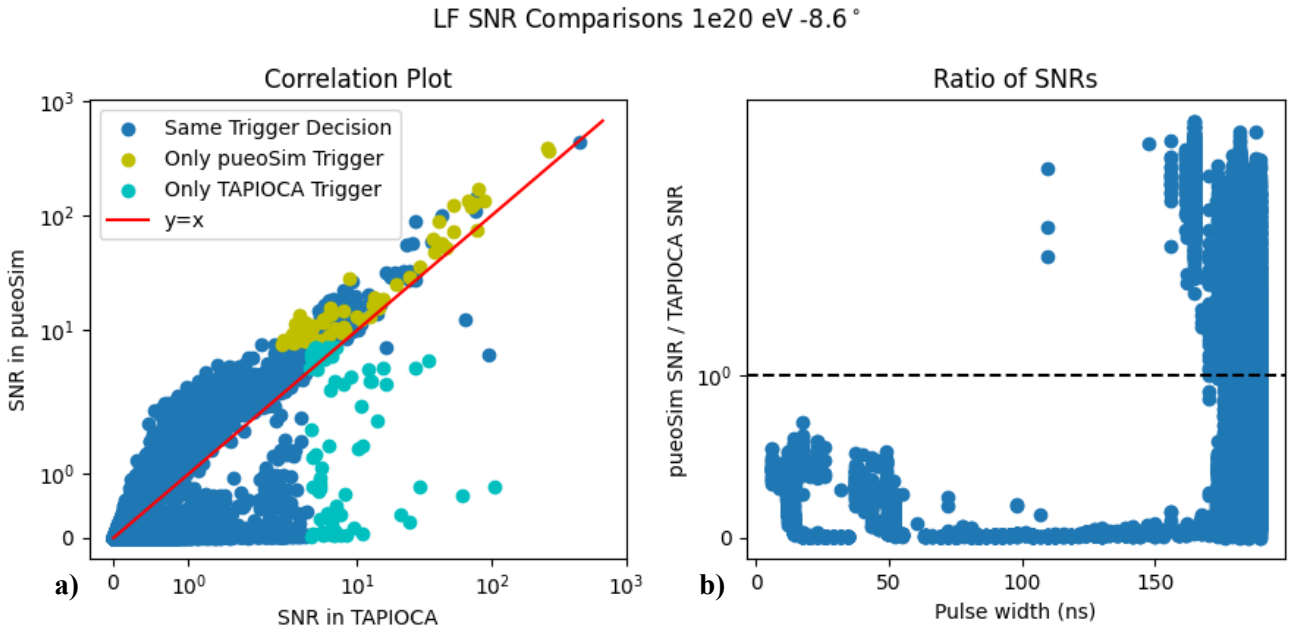

Figure 35: Comparisons of LF SNRs for events at elevation angle -8.6° and initial neutrino energy 10^{20} eV. See Figure 33 for plot descriptions. Unlike the MI, there were events that only triggered TAPIOCA's LF instrument.

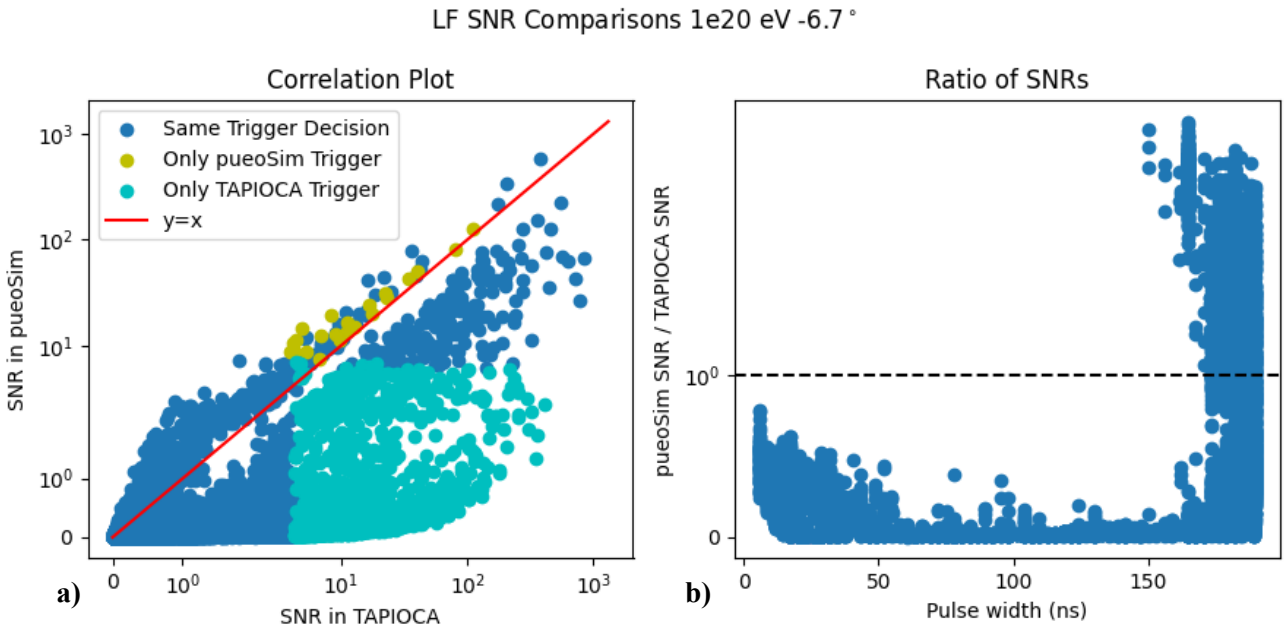

Figure 36: Comparisons of LF SNRs for events at elevation angle -6.7° and initial neutrino energy 10^{20} eV. See Figure 33 for plot descriptions.

It is a slightly different story when comparing the SNRs between the simulated LF instruments. pueoSim's LF instrument has the opposite problem as its MI; in Figures 35 and 36 it can be seen that pueoSim's LF instrument is actually decreasing many of the events' SNRs as compared to TAPIOCA. This is illustrated through many more events falling below the y=x line of Figures 35a and 36a, and below the y=1 line of Figure 35b and 36b. Nonetheless the LF instrument appears to share the same, although not as severe, issue of magnifying long duration pulses as seen in Figures 35b and 36b.

This discrepancy between pueoSim and TAPIOCA is not as visible at lower energies, such as 10^{18} eV. At lower energies, although there is still a false magnification of SNRs, the SNRs are so small to begin with that even artificially increasing their value does not put them past the trigger threshold. This results in most events still falling below threshold, not getting seen by either detector, and consequently not effecting the effective area curves. This affect can be seen in the Appendix, where parallel figures have been made of violin plots and SNR comparisons at 10^{18} eV.

5.5 Analysis and Implications

The violin plots of Section 5.3 demonstrate that the MI in pueoSim is accepting longer duration events, and more off-axis events than its counterpart in TAPIOCA. The SNR histograms of Section 5.4 show that pueoSim's MI is also producing more large SNR events than TAPICOA's MI. This increase in the number of large SNRs for pueoSim's MI can be explained by the SNR comparison plots of Section 5.4. On an event by event basis, pueoSim's MI is consistently outputting a larger SNR than TAPIOCA's MI. Additionally, this SNR magnification scales exponentially for increasing pulse width, implying that the increase in SNR can be directly

correlated with an event's pulse width. This explains the large SNRs seen in pueoSim for comparatively small SNRs in TAPIOCA: events that have long-duration electric fields are more likely to produce small SNRs in TAPIOCA and large SNRs in pueoSim.

Investigating the LF instrument's violin plots initially presents a different picture. From these figures the pueoSim's LF instrument appears to share the same distribution of accepted pulse widths and view angles as its counterpart in TAPIOCA. Additionally, the SNR histograms seem to confirm that the LF instrument is matching the distribution of SNRs between the two simulations. However, it is not until investigating the ratio of SNRs that the true behavior is exposed. pueoSim's LF instrument shares the same false amplification of low pulse width SNRs as the MI, however it simultaneously seems to decrease the SNR of more impulsive events. The magnification of long-duration SNRs and diminishment of short-duration SNRs may "balance out" the appearance of SNR histograms.

It is apparent that long-duration signals are being improperly processed in pueoSim, leading to inflated estimates of effective area. These signals are receiving artificial amplifications of SNR, leading to false triggers. Several mechanisms have been proposed to explain the cause of this SNR magnification. One explanation is that high-frequency computational noise from the electric field interpolation is being falsely amplified by the antenna response and signal chain of pueoSim's instruments. This computational noise presents itself as the rapid varying signal components in the high frequency band of Figures 17b and 17d. In reality, this high frequency band of the signal should approach 0 much more rapidly and smoothly than currently seen. These artificially large high frequency components could be amplified by pueoSim's instruments, giving false triggers.

Additionally, it has been proposed that the smaller window size of pueoSim's buffer is related to the issue. For signals that fit within 400ns, the entire pulse is captured, however information is lost for signals that extend outside of this window. When pueoSim processes these signals, a Fourier transform is utilized several times to perform frequency filtering. If there is nonzero signal at the edges of the waveform, a Fourier transform could incorrectly assume that this is a high frequency "jump" from 0 to a nonzero value, adding in false signal components. To test this theory, a project is currently in development to expand pueoSim's buffer from 1024 to 2048 samples, capturing much more of long-duration signals. Additionally, a gaussian rescaling of the waveform to smoothly reduce the signal to 0 at the edges could have the same effect.

6

Conclusion and Future Studies

Ultra-High Energy Neutrinos (UHEN) are an exciting and unexplored probe of high energy astrophysical phenomena. UHEN detectable on Earth can be produced through either Cosmogenic or Astrophysical mechanisms. While cosmogenic neutrinos are produced through the interaction of cosmic rays with the CMB, astrophysical neutrinos are directly produced in astrophysical objects such as pulsars, supernovae, and others. Although neutrinos have an extremely small cross section with most nuclei, they can be detected by utilizing the vast detector volume provided by Earth's atmosphere and ice sheets. UHEN can interact with the nuclei in the atmosphere and ice sheets to produce particle showers which give off coherent electromagnetic radiation in the radio frequency. These particle showers contain several mechanisms that produce radio, namely Askaryan emission and geomagnetic emission.

PUEO's detector arrays are specifically optimized to be sensitive to these two emission mechanisms. The MI and LF instruments utilize broadband antennas that capture a wide range of the signal power. The signal chain of each detector is designed to amplify the received signal while maintaining a low noise base. Additionally, the triggers utilize a unique beamforming system to increase the event's SNR, while only accepting the most impulsive events for more reliable reconstruction.

To estimate the experiment's sensitivity, several simulation packages have been developed that numerically model the detectors' electronics and antennas. These packages are paired with Monte-Carlo generators that simulate an array of possible neutrino events to test the detectors' response. The Monte-Carlo works by randomly sampling several parameters that determine an event's properties and using these to interpolate an electric field. This electric field

is sent to the models of the detector systems to determine if a trigger would have been declared. The calculation of these parameters and trigger results can be combined to quantify the sensitivity of the detector.

Although previous estimates have been made for PUEO's sensitivity to upgoing tau air showers, new estimates were required as significant developments have been made to PUEO's design. To generate new estimates, it was necessary to construct an interface between the tau Monte-Carlo package TAPIOCA, and the detector response package pueoSim. This interface consisted of a piping structure between the two packages, which allowed events to be transferred without saving data to disk. To match pueoSim's buffer and sampling rate, upsampling was performed on the original tau signals.

This interface and tau study produced unexpected results. Although the effective areas of pueoSim were within an order of magnitude of TAPIOCA, they differed at a consistent elevation angle. It was determined that this elevation angle generated significantly higher quantities of long-duration electric fields, which were being improperly processed by pueoSim's systems. pueoSim artificially magnifies the SNR of events with long pulse widths, causing a widening of the distributions of accepted view angles and pulse widths. This directly results in a larger calculated effective area, as there are more triggered events.

Several future studies are necessary to fully understand the direct cause of long-duration SNR magnification. It has been proposed that increasing the length of pueoSim's buffer could reduce this problem, as capturing more of the signal would lessen the chance of Fourier transform errors. However, there are still many events generated by TAPIOCA that have pulse widths that would exceed a doubled length of the buffer. A reworking of pueoSim's signal processing altogether may be necessary to completely avoid this issue. This could be achieved by

identifying the exact location that introduces artificial SNRs. If it turns out to be improper Fourier algorithms, perhaps a different Fourier algorithm would provide a more permanent solution.

Additionally, pueoSim's LF behavior is currently inadequately explained. Although it matches view angle and pulse width distributions well, for most events it is significantly decreasing the SNR compared to TAPIOCA. A useful visualization to categorize the issue may be to remake the SNR correlation plots with color coding of each event based on pulse width. The LF instrument also experiences a magnification of SNRs at long pulse widths, suggesting that this issue is independent of individual antenna responses or signal chains, but rather a processing bug in pueoSim.

Once this issue is identified and resolved, a complete analysis of PUEO's sensitivity to tau events can take place. This analysis could include the most accurate effective area and sensitivity curves to upgoing taus to date. Additionally, this analysis should investigate the reconstruction abilities of the MI antennas compared to the LF antennas. Since the MI has more antennas, it is expected to have a sharper reconstructing resolution than the LF instrument. However, the LF instrument is expected to be more sensitive to tau events. To assess the LF's value to the experiment it would be worthwhile to investigate how well the MI can reconstruct tau events when only the LF triggered on one.

Nonetheless, exciting new science results are sure to come from this experiment leading up to and after its launch date. In today's age, competitive performance of experiments can only be achieved through extensive prior predictions using numerical techniques. Performing simulation studies like those described in this thesis are crucial to the future success of scientific pursuits.

APPENDIX

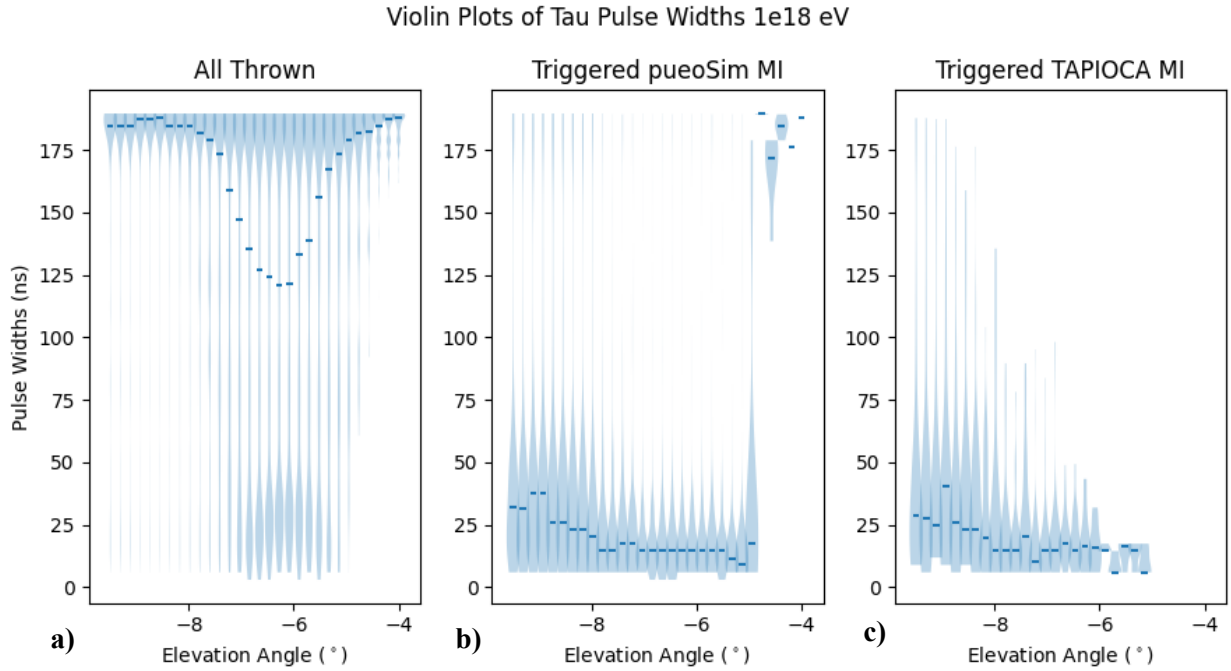

Figure A1: Violin plots for the pulse widths of upgoing tau air showers at 10^{18} eV, where **b)** and **c)** are filtered to only include MI triggered events. See Figure 27 for plot descriptions. Closer matching between simulations at 10^{18} eV than at 10^{20} eV.

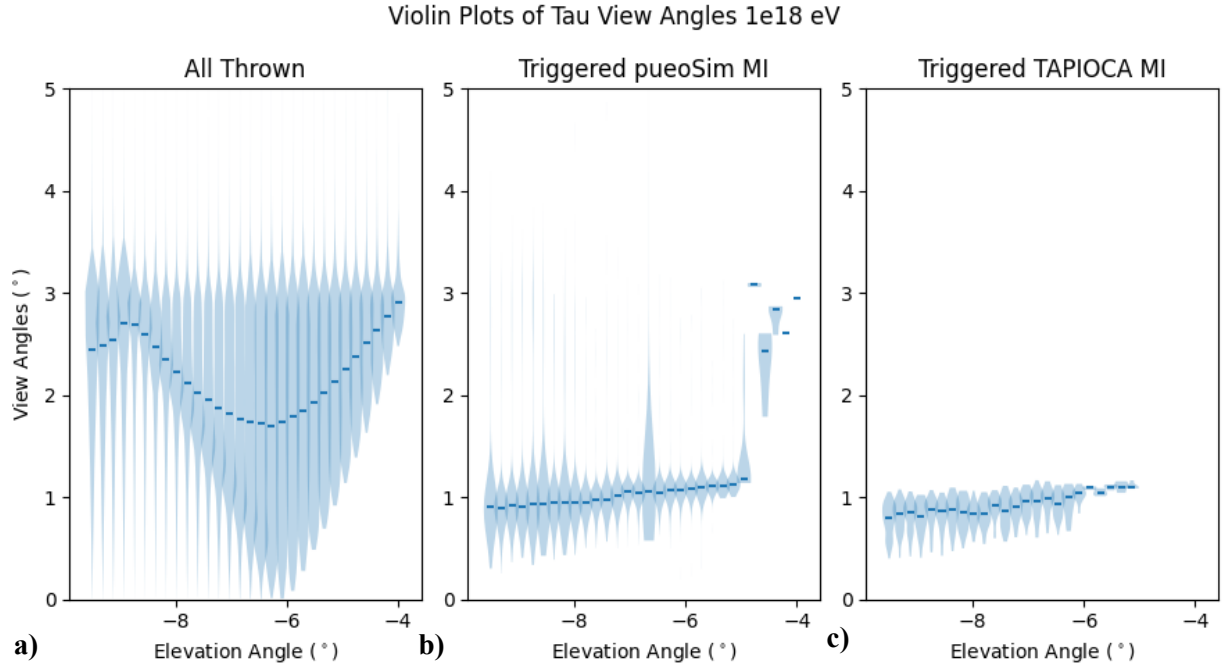

Figure A2: Violin plots for the view angles of upgoing tau air showers at 10^{18} eV, where **b)** and **c)** are filtered to only include MI triggered events. See Figure 28 for plot descriptions. Closer matching between simulations at 10^{18} eV than at 10^{20} eV.

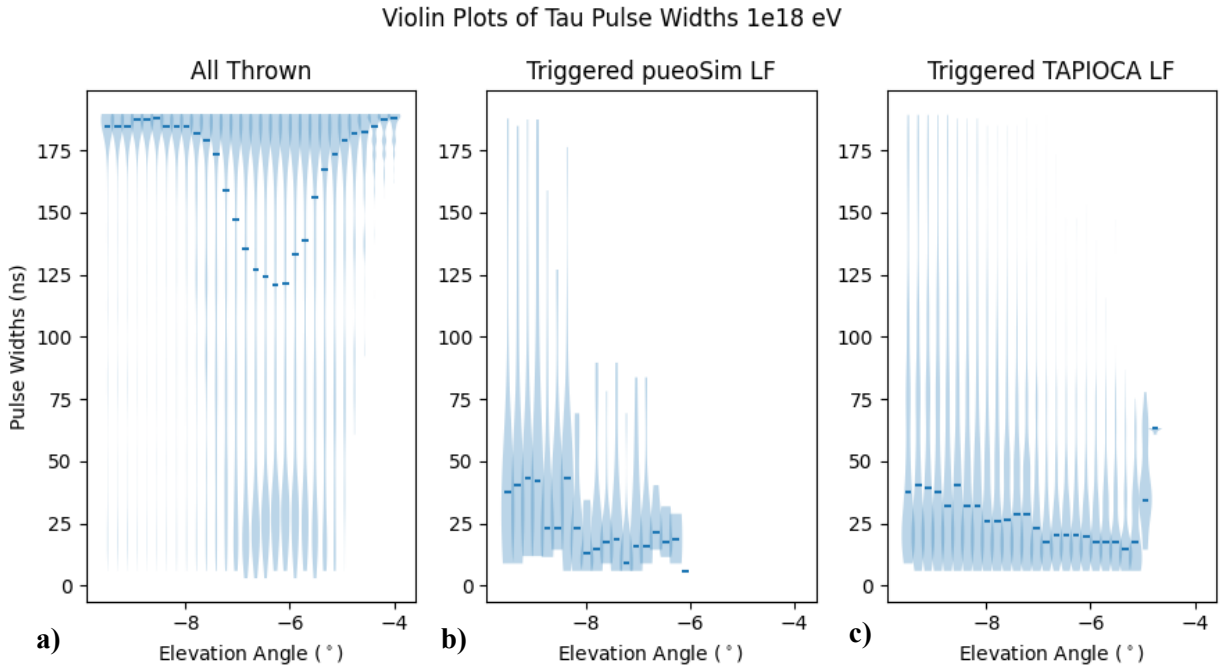

Figure A3: Violin plots for the pulse widths of upgoing tau air showers at 10^{18} eV, where **b)** and **c)** are filtered to only include LF triggered events. See Figure 27 for plot descriptions. Closer matching between simulations at 10^{18} eV than at 10^{20} eV, although pueoSim shows no triggers above -6°.

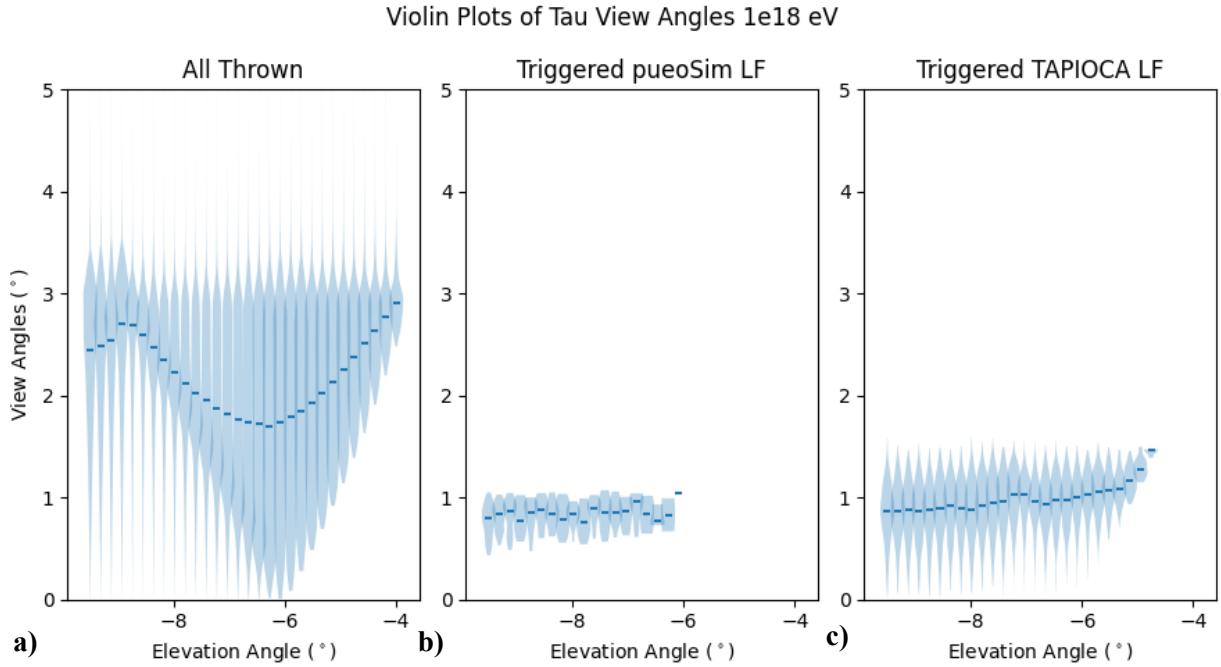

Figure A4: Violin plots for the view angles of upgoing tau air showers at 10^{18} eV, where **b)** and **c)** are filtered to only include LF triggered events. See Figure 28 for plot descriptions. Closer matching between simulations at 10^{18} eV than at 10^{20} eV, although pueoSim shows no triggers above -6°.

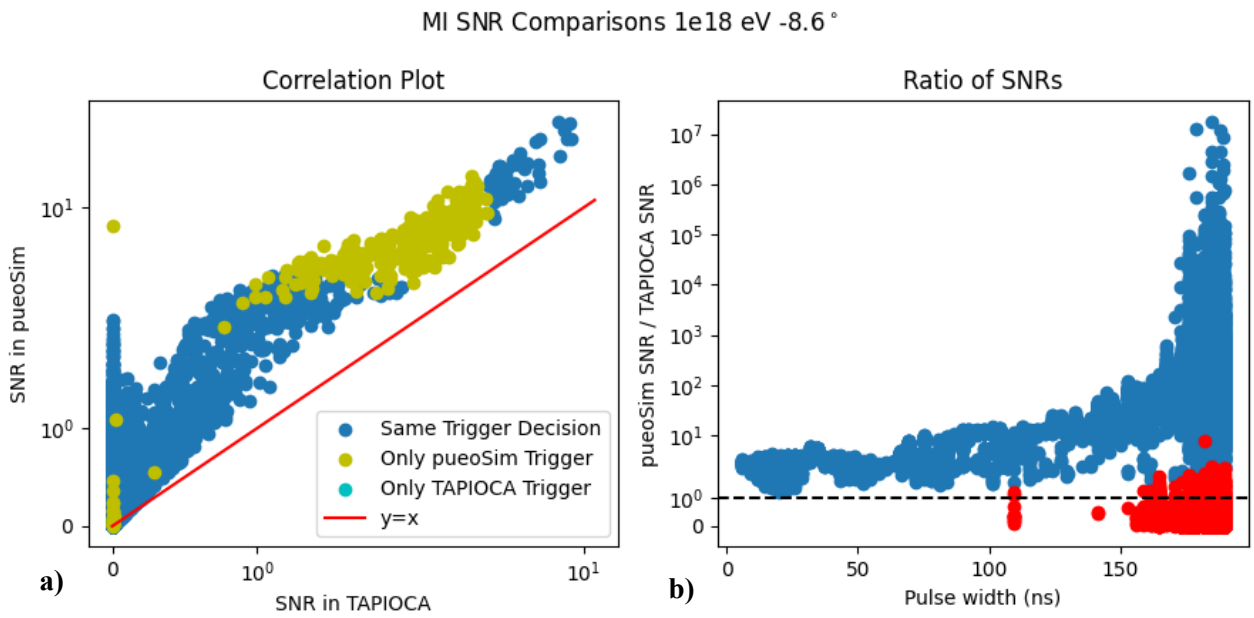

Figure A5: Comparisons of MI SNRs for events at elevation angle -8.6° and initial neutrino energy 10^{18} eV. See Figure 33 for plot descriptions. Although long pulse width magnification is still present, SNRs are too low to cross threshold and cause discrepancies in triggered events.

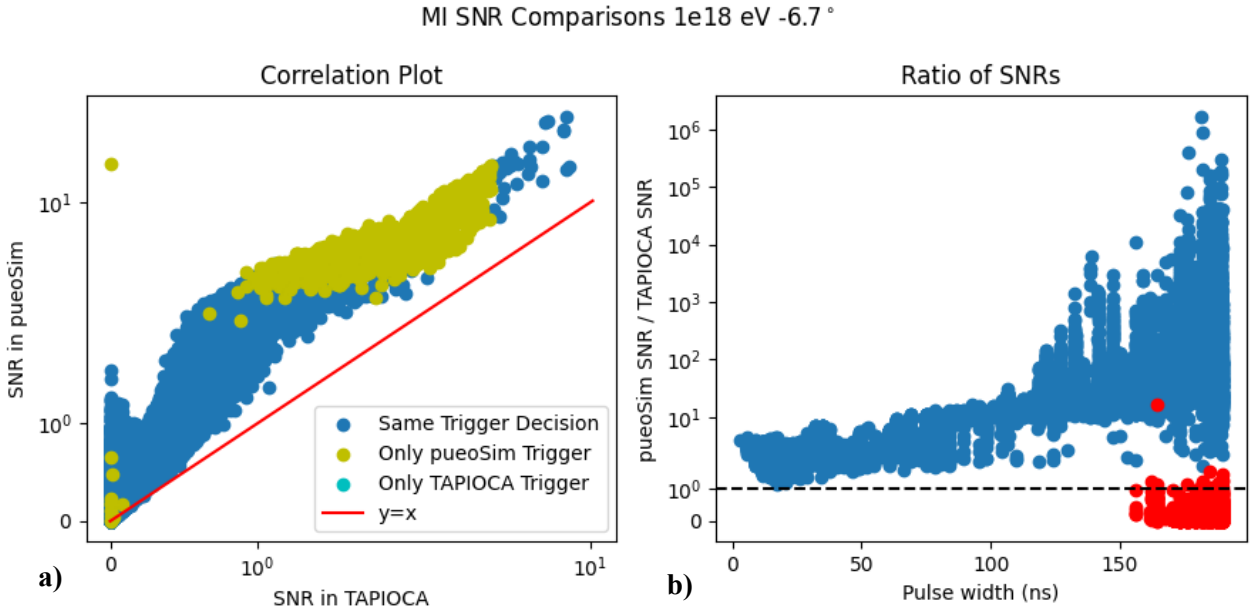

Figure A6: Comparisons of MI SNRs for events at elevation angle -6.7° and initial neutrino energy 10^{18} eV. See Figure 33 for plot descriptions.

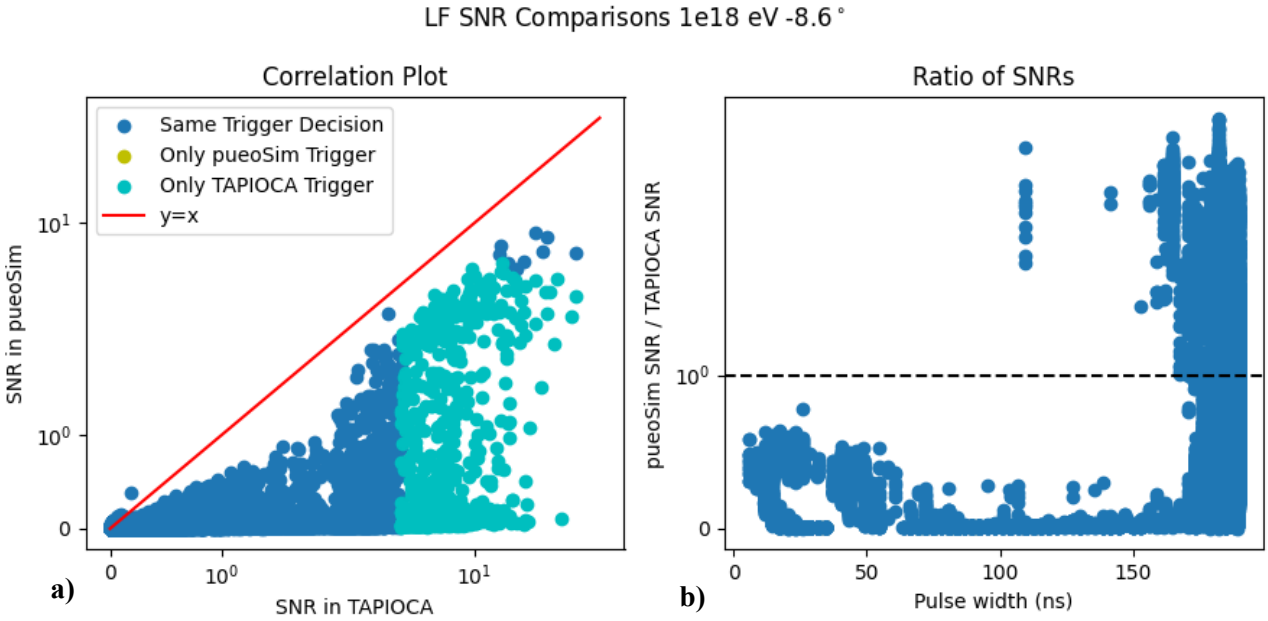

Figure A7: Comparisons of LF SNRs for events at elevation angle -8.6° and initial neutrino energy 10^{18} eV. See Figure 33 for plot descriptions. Long pulse width magnification is still present, however most SNRs are being diminished to near 0 value in pueoSim.

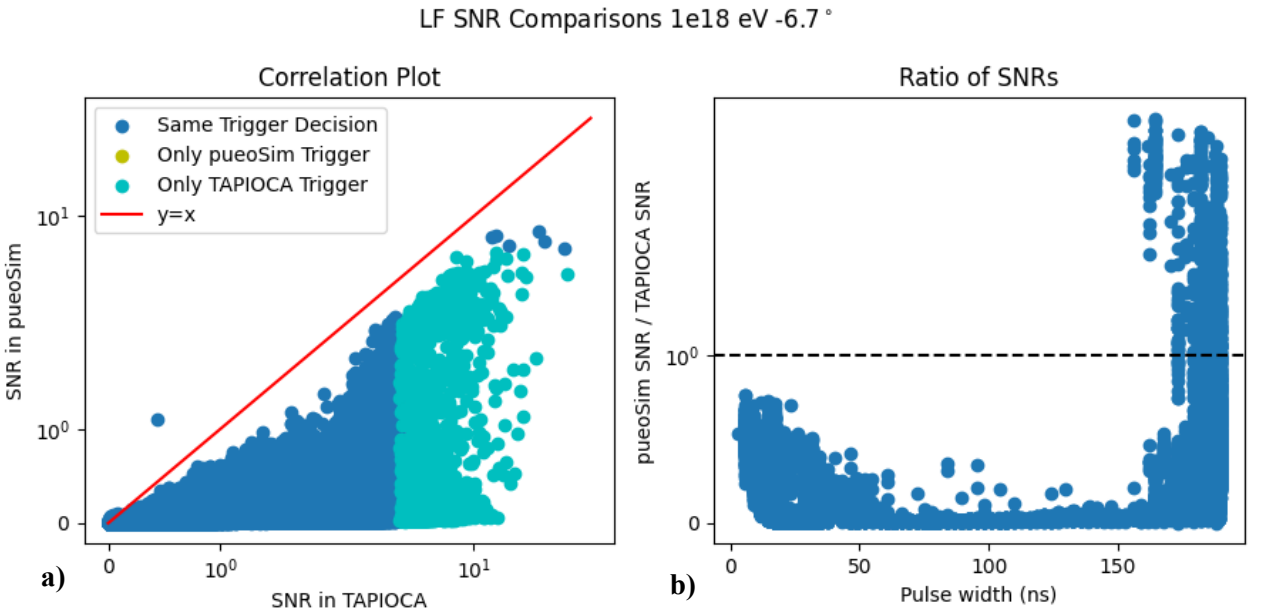

Figure A8: Comparisons of LF SNRs for events at elevation angle -6.7° and initial neutrino energy 10^{18} eV. See Figure 33 for plot descriptions.

BIBLIOGRAPHY

[1] The PUEO collaboration *et al.*, *The Payload for Ultrahigh Energy Observations (PUEO): a white paper,* JINST **16** P08035 (2021). https://doi.org/10.1088/1748-0221/16/08/P08035

[2] Glaser, C., García-Fernández, D., Nelles, A. *et al.*, *NuRadioMC: simulating the radio emission of neutrinos from interaction to detector*, Eur. Phys. J. C **80, 77** (2020). https://doi.org/10.1140/epjc/s10052-020-7612-8

[3] J. D. Bray and A. Nelles. *Minimal prospects for radio detection of extensive air showers in the atmosphere of Jupiter,* ApJ **825 129** (2016). https://doi.org/10.3847/0004-637X/825/2/129

[4] K. Greisen, *End to the cosmic-ray spectrum?,* Phys. Rev. Lett. **16** (1966) **748**.

[5] G. T. Zatsepin and V. A. Kuzmin, *Upper limit of the spectrum of cosmic rays,* JETP Lett. **4** (1966) **78**.

[6] G. A. Askaryan, *Excess Negative Charge of an Electron-photon Shower and the Coherent Radio Emission From It,* JETP **14, 2** (1961).

Dylan E. Monteiro

manonia4@gmail.com 610 716 2949

Education

The Pennsylvania State University Aug 2019 – July 2023
Schreyer Honors College
B.S. with Honors, General Physics with Mathematics Minor

Research Experience

Payload for Ultrahigh Energy Observations, Penn State May 2022 – June 2023
Advisor: Professor Stephanie Wissel
Long duration balloon experiment to observe neutrinos. Coordinated and executed simulation studies of detector sensitivity. Contributed to detector signal chain performance evaluation and design. Implemented new functionality and data transfer into detector response simulations. Contributed analysis to slides for NASA Critical Design Review.

Gopalakrishnan Group, Penn State May 2021 – Aug 2021
Advisor: Professor Sarang Gopalakrishnan
Studied single body localization in quantum chaotic systems. Simulated quantum state time evolution to analyze electron localization in quasiperiodic lattices.

LEPTOS, Penn State July 2020 – May 2021
Advisor: Professor Mikael Rechtsman
Designed new lattice structure for optical fiber cables to improve the resolution of endoscopy. Involved running numerical simulations of photon pulse propagation in differing waveguide index gradients.

Talks

APS Mid Atlantic Section Annual Meeting Dec 2022
"Trigger Correlation Schemes and Projected Sensitivity of the Low Frequency Instrument of the PUEO Experiment"

Honors/Awards

Avilés-Johnson Fellow April 2023
Sigma Pi Sigma March 2023
Phi Beta Kappa Nov 2022
Schreyer Honors College June 2021
The President's Freshmen Award March 2020

Work Experience and Involvement

Independent Tutor 2016 – present
Teaching Assistant 2018 – 19
Jazz Club, Treasurer 2022 – present
Society of Physics Students 2019-2020
Music Ensembles 2019 – present